Experimental assay of a fitness landscape on a macroevolutionary scale

Victoria O. Pokusaeva[1+], Dinara R. Usmanova[2+], Ekaterina V. Putintseva[1+], Lorena Espinar[3,4], Karen S. Sarkisyan[1,5], Alexander S. Mishin[5], Natalya S. Bogatyreva[3,4,6], Dmitry N. Ivankov[1,6], Arseniy V. Akopyan[1], Sergey Ya. Avvakumov[1], Inna S. Povolotskaya[4], Guillaume J. Filion[3,4], Lucas B. Carey[4*], Fyodor A. Kondrashov[1*]

[1]*Institute of Science and Technology Austria, Am Campus 1, 3400 Klosterneuburg, Austria.*
[2]*Department of Systems Biology, Columbia University, New York, 10032, NY, USA.*
[3]*Bioinformatics and Genomics Programme, Centre for Genomic Regulation (CRG), 88 Dr. Aiguader, 08003 Barcelona, Spain.*
[4]*Universitat Pompeu Fabra (UPF), 08003 Barcelona, Spain.*
[5]*Shemyakin-Ovchinnikov Institute of Bioorganic Chemistry, Miklukho-Maklaya 16/10, 117997 Moscow, Russia.*
[6]*Laboratory of Protein Physics, Institute of Protein Research of the Russian Academy of Sciences, Pushchino, Moscow region, Russia*
[+]*Equal contribution*
[*]*Authors for correspondence*

Characterizing the fitness landscape, a representation of fitness for a large set of genotypes, is key to understanding how genetic information is interpreted to create functional organisms. Here we determined the evolutionarily-relevant segment of the fitness landscape of His3, a gene coding for an enzyme in the histidine synthesis pathway, focusing on combinations of amino acid states found at orthologous sites of extant species. Just 15% of amino acids found in yeast His3 orthologues were always neutral while the impact on fitness of the remaining 85% depended on the genetic background. Furthermore, at 67% of sites, substitutions are under sign epistasis, having both strongly positive and negative effect in different genetic backgrounds. 46% of sites were under reciprocal sign epistasis. Sign epistasis affected few genotypes but involved interaction of multiple sites, shaping a rugged fitness landscape in which many of the shortest paths between highly fit genotypes are inaccessible.

Predicting function and fitness of organisms from their genotypes is the ultimate goal of many fields in biology, from medical genetics to systems biology to the study of evolution[1-5]. Among the conceptual frameworks for understanding the genotype to phenotype connection is the fitness landscape, which assigns a fitness (phenotype) to every possible genotype (sequence) of a gene or genome under consideration[4,6]. The recognition of the importance of the fitness landscape stimulated the development of a variety of theoretical approaches to its description, including its general shape and epistatic interactions between alleles, a key property which determines the complexity of the fitness landscape (see [ref. 4] and references within). Before the advent of next-generation sequencing, experimental assays of the fitness landscape were few and could not address the issue at the sequence level. Recently, large-scale experimental assays described the shape of the fitness landscape a few mutations away from a local fitness peak (see [ref. 7-10] and references within). Also, some assays involving a smaller number of genotypes considered combinations of mutations with established functional[11-16] or evolutionary[17-22] significance.

Empirical evidence of the nature of large-scale fitness landscapes mostly comes from the study of genotypes incorporating random mutations[4,7-10], the majority of which are deleterious[7-10,23]. Thus, our present knowledge of fitness landscapes is primarily driven by the study of deleterious mutations and their interactions, although local adaptive trajectories have also been considered[2,4,16,24-26]. Deleterious mutations were found to engage in synergistic epistasis,

whereby the joint effect of multiple mutations was stronger than the sum of their individual effects[4,7-10,16]. Furthermore, sign epistasis among random mutations was mostly rare[5,7-10,16,27], although some of these conclusions differ from study to study (*e.g.* see [4,27]).

Unfortunately, there are fundamental limitations to assaying the fitness landscape on a large or macroevolutionary level with random mutation libraries. The number of genotypes underlying the fitness landscape is the combinatorial set of all amino acids across the length of the protein[4,6]. For example, for the 220 amino acid protein coded by the His3 gene in *Saccharomyces cerevisiae*, the fitness landscape is a 220 dimensional genotype space with 20^{220} different possible sequences. Such immense spaces are both computationally and experimentally intractable. Fortunately, it may not be necessary to survey all genotypes to study the evolutionary-relevant section of the fitness landscape. Because the vast majority of mutations in protein sequences are deleterious[23], a randomly sampled protein sequence is non-functional[28,29].

Here we propose an evolutionary approach for assaying fitness landscapes on a macroevolutionary scale in a high-throughput manner that avoids the random sampling of mostly non-functional sequences. The functionally and evolutionarily relevant section of the fitness landscape can be represented by the combination of extant amino acid states, those found in extant species. This approach, applied previously on a limited scale[17-22] mitigates the problem of exploring a prohibitively large fitness landscape while highlighting the relationships between evolutionarily-relevant genotypes **(Fig. 1a)**. Crucially, substitutions that have been fixed in evolution are fundamentally different from random mutations, the former are either neutral or beneficial in at least some genetic contexts and represent the driving force of molecular evolution, while the latter are mostly deleterious and are primarily relevant on a microevolutionary scale. Therefore, current empirical data do not shed much light on the impact of interactions between substitutions that fixed in the course of evolution by natural selection. Combinations of extant amino acid states allow one to assay a much wider functionally relevant area of the sequence space than approaches based on random mutagenesis of a single sequence (**Fig. 1b,c**).

Estimating fitness of evolutionary-relevant genotypes

We studied His3, a gene coding for imidazoleglycerol-phosphate dehydratase (IGPD, His3p), an enzyme essential for histidine synthesis. In a multiple alignment of His3 orthologues from 21 yeast species we identified 686 extant amino acid states (**Supplementary Information 1**), which were evenly distributed across the His3p structure (**Fig. 1d**). These 686 substitutions, which occurred over the course of ~400 million years of evolution[30] (**Fig. 1b,c**) correspond to ~10^{83} sequences, even a tiny fraction of which would be too many to survey. Thus, we sectioned His3 into 12 independent segments such that the full combinatorial set of substitutions that have occurred in His3 during yeast evolution comprised 10,000-100,000 genotypes per segment (see **Methods** and **Supplementary Fig. 1a**). The 12 segments were of similar length, constrained by the molecular methods employed for library construction (see **Methods**), and covered a diverse range of secondary structures and functional elements (**Supplementary Fig. 1c**). For each of the 12 segments of His3 we performed an independent experiment surveying its fitness landscape. For each segment we used degenerate oligonucleotides to construct genotypes consisting of combinations of amino acids present in extant His3 sequences, and determined the fitness conferred by these genotypes by expressing them in a Δ*his3* strain of *S. cerevisiae* and measuring the rate of growth **(Supplementary Fig. 1b)**. This way we assayed the fitness landscape of the genotype space that was traversed over the course of the last ~400 million years of evolution[30].

Across 11 experiments we measured fitness for a total of 4,018,105 genotypes (875,151 unique amino acid sequences) with high accuracy. Of these, 422,717 consist solely of

combinations of extant amino acid states from His3 orthologues, while the remaining genotypes incorporate other amino acid substitutions (**Supplementary Table 1** and **Methods**). For one segment, 9, the accuracy of our experiment was low, and it was not used in cumulative analyses. For each segment we measured fitness for 60% - 99.8% of all possible genotypes from the combinatorial set of selected extant amino acid states found in 21 yeast species and a smaller fraction of combinations found across all domains of life (**Supplementary Table 1**), characterizing the evolutionary relevant fitness landscape **(Fig. 1b)**. For segment 3 for instance, 11 out of 17 amino acid sites had more than one extant amino acid state: L145=2, L147=2, Q148=3, K151=2, V152=2, D154=3, L164=3, E165=4, A168=2, E169=4, A170=4, with the full yeast combinatorial set consisting of 2*2*3*2*2*3*3*4*2*4*4 = 55,296 genotypes out of which we determined the fitness for 48,198, or 87% of the possible yeast extant states combinations in our library.

A substantial proportion of combinations of extant amino acid states led to genotypes with low fitness (**Fig. 2, Fig. 3a,b, Supplementary Fig. 2**), an observation that takes into account the false discovery rate in our data (**Supplementary Table 1**). This observation could be explained by i) some extant amino acids having a universally deleterious effect, ii) some amino acid states exerting a negative effect on fitness because of intergenic interactions with other *S. cerevisiae* genes, or iii) by epistatic interactions between the extant amino acid states within His3[31]. We exclude the possibility that some extant amino acid states had a universally deleterious effect because no extant amino acid states were present only in unfit genetic backgrounds, genotypes conferring a fitness of zero (**Fig. 3c**). We exclude the possibility that some extant amino acid states disrupt intergenic interactions because the complete His3 coding sequences from extant species fully complemented a His3 deletion in *S. cerevisiae* (**Supplementary Fig. 3c**). Thus, the observed genotypes with low fitness can only be explained by epistatic interactions among extant amino acid states within the His3 gene in the same or different segments. Remarkably, 85% (330/389) of substitutions between extant amino acid states had substantially different effects on fitness in different backgrounds (**Fig. 3d**). By contrast, only 15% of amino acid substitutions that occurred in His3 evolution are truly neutral, in the sense that they do not exert strong influence on fitness in any genetic background. Three quarters of the universally neutral substitutions were observed in the disordered region of the protein (44/59). Thus, the His3 fitness landscape across the 11 segments with high accuracy was strongly influenced by epistasis on a macroevolutionary scale, i.e. the impact of an extant amino acid state on fitness often depends on the background in which it occurs[31-34]. An epistatic fitness landscape is rugged in the sense that evolving genotypes must avoid fitness valleys that emerge through deleterious combinations of amino acid states that may also be found in fit genotypes[18,19,34-36]. Characterizing the ruggedness and the mechanisms that determine the underlying epistasis becomes the primary challenge in understanding the fitness landscape of His3.

Unidimensional epistasis of the His3 fitness landscape

The ruggedness of the fitness landscape can be characterized by different measures of complexity of the underlying epistatic interactions. In the simplest case, epistasis may be unidimensional, in the sense that the fitness landscape can be described as a function of an intermediate variable, the fitness potential[37-39]. The fitness landscape is a function from the space of genotypes to fitness. In analogy with a scalar field, we can characterize the ruggedness of this function with standard measures of complexity if genotypes are arranged in a linear space. The simplest case is that of a linear predictor called the fitness potential: $p = c_1x_1 + c_1x_2 + \ldots + c_nx_n$, where c_i is a coefficient and x_i is a binary variable that signifies the presence (1) or absence (0) of a given amino acid at a given position. By definition, e^p describes a non-epistatic fitness landscape because the effect of every substitution is multiplicative and it depends only on the

associated c. Any other function of p leads to epistasis. If the $f(p)$ function is "simple", meaning that is has a small number of local extremas, such as a bimodal function, the epistasis is called unidimensional[39]. The limitation of simplicity of $f(p)$ is necessary because any function $f_0(x_1, \ldots, x_n)$ can be represented by a function $f'(p)$ and choosing appropriate coefficients $c_1, \ldots, c_n$ in p. Thus, a simple $f(p)$ leads to unidimensional epistasis because the entire genotype space can be reduced to a single dimension[39].

To quantitatively determine how well fitness differences between genotypes can be explained by unidimensional epistasis we used a deep learning approach to estimate the coefficients c for each allele x in the fitness potential and determine the best unidimensional function of p that best approximated the fitness landscape. We used a dense neural network architecture composed of three layers. Each neuron in the architecture performed a linear transformation of its input and then applied a nonlinear (sigmoid) function. Hence, by using one neuron in the first layer we obtained a linear combination of the contributions of each amino acid state to fitness potential, which was then non-linearly mapped to fitness by the three layers of the neural network architecture (see **Methods**; **Supplementary Fig.4**). Ten segments were described by a threshold function in which organismal fitness remains constant with decreasing fitness potential and then is rapidly reduced to lethal after a certain threshold (**Fig. 4a**). The ability of the cliff-like threshold fitness function[40] to predict fitness from genotype varied between the His3 segments from near perfect (r^2=0.97) in segment 7, to relatively poor (r^2=0.44) in segment 5 (**Supplementary Fig. 5**). Thus, while the fitness landscape of His3 is approximately unidimensional for some segments, it has a higher degree of complexity for others.

Ruggedness and multidimensional epistasis of the His3 fitness landscape

Ruggedness is a general property of fitness landscapes that quantifies the accessible paths of high fitness that connect fit genotypes[41-43]. A path between highly fit genotypes is inaccessible when one of the intermediate genotypes has low fitness[6,20-22,41,44] (*e.g.* for genotypes AB and ab, the intermediate are aB and Ab). Such instances also manifest in sign epistasis on the fitness landscape, that the same substitution may be beneficial or deleterious when occurring in a different genetic background[44,45]. To quantify the ruggedness of the His3 fitness landscape we identified instances of sign epistasis: substitutions between extant amino acid states that were strongly beneficial or strongly deleterious (change in fitness of > 0.4 in absolute value) depending on the background in which they occurred[44]. Some of these instances may be due to miscalled fitness of very few genotypes. Therefore, we considered a pair of extant amino acid states to be under sign epistasis only when sign epistasis was observed in a statistically significant number of different genetic backgrounds (see **Methods**).

An example of sign epistasis is the substitution C141S in the second segment that had an opposite effect on fitness depending on amino acid at site 143 (I, V or T). The substitution I143T in turn exhibits sign epistasis depending on the amino acid at site 163 (F, I, V or L) **(Fig. 5a)**. These epistatic interactions can be represented by a graph in which nodes represent a pair of extant amino acid states at a specific site and nodes are connected by edges if strong sign epistasis has been detected between them (C141S - I143T - I163F) **(Fig. 4b)**. We found that 86 out of 128 (67%) sites in our library exhibit sign epistasis and 46% (59/128) exhibit reciprocal sign epistasis. Most sites showed a sign epistatic interaction with multiple other sites (**Fig. 5c,d**) demonstrating that, although sign epistasis affects few genotypes, it leads to a fitness landscape that requires the interaction of multiple sites for proper characterization.

The complexity of interaction of sites can be estimated by using the graph of sign epistasis where vertices represent a substitution and edges connect vertices with sign epistasis between them. If only few substitutions display sign epistasis then such a graph would signify

that the fitness landscape is relatively smooth, alternatively, a highly-interconnected graph of such interactions signifies a more rugged landscape[4,5,41-43]. To measure the relative fitness complexity, we used the maximum clique size of a graph, which approximates the maximum number of simultaneously interacting substitutions. In our data, this measure ranged from two to seven depending on the segment (**Supplementary Fig. 6**). The ruggedness of the fitness landscape of His3 is high for most segments, such as segment 5, where it is necessary to consider the simultaneous interaction of at least seven sites to accurately predict the fitness of genotypes consisting of extant amino acid states at these sites[38,40].

Sign epistasis can appear when fitness is described by a unidimensional function of the fitness potential, for example, when the fitness landscape is a unimodal function with an optimum in an intermediate range of the fitness potential[41,45]. However, sign epistasis may also be a sign of multidimensional epistasis, when a unidimensional function of the fitness potential cannot fully describe genotype fitness[39]. Many genotypes were predicted poorly by a unidimensional function of the fitness potential (**Supplementary Fig. 5a**). Two lines of evidence suggest that such genotypes reveal the presence of multidimensional epistasis. First, genotypes with a higher number of substitutions influenced by sign epistasis were less well-predicted by a unidimensional fitness function (**Fig. 4c and Supplementary Fig. 7b**). Second, we explain a larger fraction of genotypes by using a more complex neural network architecture accommodating multiple fitness potentials instead of one. We found that increasing the amount of neurons in the first layer of the neural network architecture, which is equivalent to increasing the number of independent fitness potentials, gradually improves the prediction power of the obtained models for most of the segments (**Fig. 4d**). Thus, adding dimensions to the function of fitness potential increases the prediction power of the model. For example, for a two-dimensional case fitness was described by $f_1(p_1, p_2)$ with $p_1 = a_1x_1 + a_1x_2 \ldots a_nx_n$ and $p_2 = b_1x_1 + b_1x_2 \ldots b_nx_n$. For several His3 segments, a fitness function with multiple underlying fitness potentials described the fitness landscape more accurately than a simple unidimensional function of a single fitness potential (**Supplementary Fig. 7a**). For instance, for these segments, fitness function of two fitness potentials described the shape with a higher degree of accuracy than a function of a single fitness potential (**Fig. 4d,e**). By contrast, epistasis in segment 7 is entirely unidimensional (**Fig. 4d,e and Supplementary Information 2**); we do not see any improvement in the model's predictive power when adding extra dimensions.

Evolutionary trajectories on the His3 fitness landscape

On a smooth fitness landscape, evolution can proceed along any of the evolutionary paths connecting two fit genotypes, as none of the intermediate genotypes confer low fitness (see Box 2 in [46]). Alternatively, the fitness landscape is rugged when it contains non-connected fitness peaks, such that there are no viable paths between some pairs of genotypes that confer high fitness[4,5]. In other words, the presence of deleterious intermediate genotypes between highly fit ones leads to inaccessibility of some evolutionary trajectories between extant or ancestral sequences[6,20-22,44]. The simplest explanation for the substantial ruggedness of the landscape observed in many of the His3 segments lies in the unidimensional threshold fitness function (**Fig. 6a**). On a threshold function a combinations of substitutions, all of which are neutral in some genetic backgrounds, can take a genotype beyond the fitness threshold through their additive effect on fitness potential, making some genotypes inaccessible for evolution (**Fig. 6a**). Between any two fit genotypes, the fraction of intermediate genotypes that are unfit depends on the fitness potential of the two parental genotypes (**Fig. 6b**). Evolution between two fit genotypes with high fitness potential can proceed unhindered because all intermediate genotypes also have high fitness potential and, consequently, high fitness. Conversely, when both fit genotypes are located close to the threshold, many of the intermediate genotypes between them have low fitness and many evolutionary paths between them are inaccessible (**Fig. 6c**). Thus, the

258 cliff-like threshold fitness function is the major determinant of the observation that not all paths
259 between two fit genotypes are accessible to evolution (**Fig. 6b**). We find that unfit intermediate
260 genotypes are in genetic proximity with each other and are on a limited number of paths; the
261 fraction of inaccessible paths is smaller than if the same number of unfit genotypes were
262 distributed randomly in genotype space (**Fig. 6d,e**).
263
264 The effect of synergistic epistasis dominates the His3 fitness landscape, affecting over
265 85% of amino acid substitutions from our library that occurred in His3 evolution. This
266 synergistic epistasis may reflect the free energy of the protein[10,47,48], as evidenced by a
267 correlation between the fitness potential and the impact of substitutions on the free energy of
268 His3p (**Supplementary Fig. 8**). Similarly, instances of sign epistasis may also be explained by
269 changes in protein stability; for example, in the 143T background C141S increased fitness and
270 also had a positive effect on stability (**Fig. 5b)**. Consistent with protein stability contributing to
271 the observed sign epistasis we find that sites that exhibited reciprocal sign epistasis are close
272 together in the His3p structure **(Supplementary Fig. 8)**. However, an additive contribution to
273 free energy can lead only to a unidimensional fitness function[47], indicating that other non-
274 additive mechanisms, such as catalytic activity or inter-subunit interactions, or a non-additive
275 model of free energy, must be responsible for the multidimensionality of the His3 fitness
276 landscape.
277
278 **Inference of inter-segmental epistatic interactions in the His3 gene sequence**
279
280 Epistasis may be caused by interaction among positions within a segment (intra-
281 segmental epistasis) or by interaction of the segment with the rest of the *S. cerevisiae* His3
282 sequence (inter-segmental epistasis). The contribution of inter- versus intra-segmental
283 interactions can be decoupled. Given two fit genotypes (*e.g.* ABC & abc in one His3 segment),
284 any unfit intermediate states (*e.g.* aBc in the same His3 segment) must be due to intra-segmental
285 epistasis because the rest of the protein remains constant. For each segment we took as a
286 measurement of intra-segmental epistasis all pairs of fit genotypes and calculated the proportion
287 of unfit intermediate genotypes as a function of the Hamming distance between the two fit
288 genotypes. We then compared this proportion with the total proportion of all unfit genotypes as a
289 function of Hamming distance from *S. cerevisiae*, a measurement that includes both inter- and
290 intra-segmental epistasis. We found three times more inter-segmental than intra-segmental
291 epistasis **(Supplementary Fig. 9)**, likely because a single segment provides a much smaller
292 target space for interactions than the entire His3 protein. The proportion of sites under epistatic
293 interactions increased exponentially with Hamming distance (**Supplementary Fig. 9**), analogous
294 to Orr's snowball, the accumulation of genetic incompatibilities in the course of speciation[31,49].
295
296 **Conclusions**
297
298 The concept of the fitness landscape introduced by Sewall Wright (Figures 1 and 2 in [6])
299 is an indispensable tool for understanding multiple biological phenomena[1-5]. Experimental high-
300 throughput assays of random mutations have begun to unravel some local properties of fitness
301 landscapes[4]. Here, we described a fitness landscape on a macroevolutionary scale by focusing on
302 amino acid states that have been put through the sieve of natural selection. We found that only
303 15% of substitutions that fixed in the evolution of His3 are universally neutral. For the remaining
304 85%, substitutions from His3 evolution had a profound influence on each other's effect on
305 fitness, providing an experimental confirmation that epistasis is one of the defining features of
306 molecular evolution[33]. Substitutions that occur in evolution have properties vastly different from
307 those of random mutations, which are mostly deleterious[23]. Therefore, the way in which
308 combinations of extant amino acid states affect fitness may also be different from that of
309 combinations of random mutations. Unexpectedly, we found that the interaction of extant amino

acid states was dominated by synergistic epistasis in a manner similar to that previously found for random mutations[7-10,16]. However, the accumulation of random mutations leads to low fitness much faster than the accumulation of extant amino acid states (compare Figure 2 from [16] and Figure 3b from [10] to **Fig. 2a**).

The experimental data showing that 85% of amino acid states found in extant species confer low fitness in a different genetic background lends strong support to the notion that epistasis is a key factor in protein evolution[31,33]. We showed that the fitness landscape of several segments of the His3 gene cannot be reduced to a single unidimensional forms of epistasis, with a function of multiple fitness potentials providing a more accurate description of the fitness landscape. By contrast, large-scale fitness landscapes incorporating multiple random mutations away from the wildtype sequence in a constant test environment have not displayed evidence of multidimensional epistasis[8-10,16]; however, it appears to be a more prevalent factor among substitutions that have been subject to positive selection[12-16,18-22,34-36]. We also found that up to 67% of sites with an extant amino acid state were influenced by sign epistasis, resulting in a rugged fitness landscape and a limited number of fitness ridges connecting extant sequences for most His3 segments. Overall, the evolutionary-relevant section of the His3 fitness landscape is best described as a fitness ridge, with the crest of the ridge defined by a fitness potential. In some cases, the crest is multidimensional requiring several independent underlying fitness potentials. Evolution can proceed unhindered along the crest **(Fig. 6a,c)**, however, pathway availability declines rapidly when evolution proceeds close to the edge of the fitness ridge.

Acknowledgements

We thank Ben Lehner for a thorough study of the concept behind our experiments and Julia Domingo for technical assistance with preliminary analysis of our data. Jochen Hecht of the CRG Genomics Unit and Svetlana Belogorodtdeva and Roman Belogorodtsev provided technical assistance. The work was supported by HHMI International Early Career Scientist Program (55007424), the MINECO (BFU2012-31329, BFU2012-37168, BFU2015-68351-P and BFU2015-68723-P), Spanish Ministry of Economy and Competitiveness Centro de Excelencia Severo Ochoa 2013-2017 grant (SEV-2012-0208), the Unidad de Excelencia María de Maeztu funded by the MINECO (MDM-2014-0370), Secretaria d'Universitats i Recerca del Departament d'Economia i Coneixement de la Generalitat AGAUR program (2014 SGR 0974), the CERCA Programme of the Generalitat de Catalunya, Russian Foundation for Basic Research grant (18-04-01173), the European Union's Horizon 2020 research and innovation programme under the Marie Skłodowska-Curie programme (665385) and the European Research Council under the European Union's Seventh Framework Programme (FP7/2007-2013, ERC grant agreement 335980_EinME and Synergy Grant 609989).

Author contribution. ISP, LBC and FAK conceived the general approach of the study. FAK, LBC, VOP, LE and GJF participated in detailed experimental design. VOP, DRU and EVP spearheaded the experiment, data analysis and main data interpretation, respectively. LE performed a large fraction of the experimental work. AVA and SYaA participated in working on dimensionality. KSS, ASM, NSB, DNI and GJF participated in data analysis. LBC and FAK wrote the draft.

Methods

Data access

The raw and processed data have been submitted to the NCBI Gene Expression Omnibus (GEO;http://www.ncbi.nlm.nih.gov/geo/) under accession number GSE99990. A virtual machine containing a running version of the data processing pipeline is available as a Docker image

https://hub.docker.com/r/gui11aume/epi/. The scripts to reproduce the figures are on Github at https://github.com/Lcarey/HIS3InterspeciesEpistasis.

Study design

The His3 gene was selected for three principal reasons, it is short, conditionally essential and was not known to be involved in protein-protein interactions. Studying 20^{220} variants of His3 is impossible, thus, we have chosen an approach to survey the fitness landscape in a manner that would elucidate the area most relevant to His3 evolution while managing the technical limitations of our experimental design. We considered amino acid states found in extant species, focusing on yeast species, which translated into a full combinatorial set of $\sim 10^{83}$ unique genotypes. Technically it is feasible to measure fitness of up to 100,000 unique genotypes in a single growth experiment. Therefore, we split the His3 gene into 12 independent segments such that the full combinatorial set of extant amino acid states from 21 yeast species in each segment was 10,000 – 100,000 genotypes. We then considered the combinatorial library for each segment in an independent growth experiment, which allowed us to study a tractable section of the sequence space while considering trajectories across a vast part of the space connecting extant species (**Fig. 1a**). We constructed these combinations in 12 plasmid libraries and transformed them into a haploid His3 knockout *S. cerevisiae* strain. Growth rate (fitness) of yeast carrying different mutations in His3 was measured using serial batch culture in the absence of histidine.

We split the His3 gene sequence into segments in a manner agnostic to the structure of the His3 protein (**Supplementary Fig. 1a**). For technical reasons, a segment consisted of two variable regions with a constant region between them (**Supplementary Fig. 1b**). All growth experiments were performed independently for each segment, with the exception of one experiment on a limited group of genotypes from each segment which was done for the normalization of fitness values across different segments (**Supplementary Fig. 3**).

As a control, we measured the rate of growth of *S. cerevisiae* whose entire His3 gene sequence came from another distant species. We found that the replacement of an entire gene sequence of His3 leads to wild-type rates of growth of *S. cerevisiae* even when the His3 sequence comes from very distant yeasts, as far as *S. pombe* (**Supplementary Fig. 3**). Therefore, His3 appears to be an independent unit of the fitness landscape and is a good model for the study of fitness landscapes of an isolated gene.

Measuring fitness

Plasmid construction

The His3 open reading frame of *S. cerevisiae* was PCR amplified with its regulatory region from 622 base pairs (bp) upstream of the open reading frame (ORF) to 237 bp downstream of the ORF, using primers 126 and 127 (see **Supplementary Table 1**) from the wild-type prototroph strain FY4. The PCR product was cloned into vector pRS416 using Gibson assembly (NEB, E2611S). The His3 orthologues from other species were amplified from genomic DNA using designed primers (**Supplementary Table 1**) and were cloned into the vector pRS416_his3, replacing the ORF of *S. cerevisiae* by Gibson assembly (NEB, E2611S). Since the His3 orthologue from *A. nidulans* contains an intron, the whole open reading frame was initially cloned into the vector, and the intron was later removed by PCR-amplifying the whole plasmid without this sequence, followed by recircularization.

Genomic DNA extraction

Genomic DNA from fungi (*Saccharomyces cerevisiae, Saccharomyces bayanus, Candida glabrata, Saccharomyces castellii, Kluyveromyces lactis, Eremotheciumgossypii, Debaryomyces hansenii, Lodderomycese longosporus, Aspergillus nidulans, Schizosaccharomyces pombe, Candida guilliermondii, Saccharomyces kluyveri, Kluyveromyces waltii*) was extracted using MasterPure™ Yeast DNA Purification Kit according to the manufacturer's instructions (Epicentre, MPY80200).

413
414 *Mutant library construction*
415 Twelve independent mutant libraries, each for different regions of His3 **(Supplementary**
416 **Table 1)**, were generated based on the results of multiple alignment of His3 orthologues. The
417 alignment was built using the ClustalW alignment feature of the MEGA 6.0 software package[50]
418 and user-corrected.
419 Mutant libraries were constructed by fusion-PCR, leaving two variable regions separated
420 by a constant region. For each library, two contiguous fragments of His3 were amplified
421 independently, using 1 µg of *S. cerevisiae* (strain FY4) genomic DNA in separate Phusion
422 polymerase reaction mixes (Thermo Fisher Scientific, F530S) in GC buffer. For each PCR, one
423 of the primers was a degenerate oligonucleotide with a constant part at the 5' end required for
424 the fusion-PCR; the other primer was either 126 or 127. The degenerate primer approach led to
425 the integration of non-extant amino acid sequences due to the redundancy of the genetic code.
426 Consider the amino acid Phe in *S. cerevisiae* coded by the codon TTT. When incorporating an
427 extant orthologous state Trp (TGG) two independent T -> G nucleotide mutations will be
428 incorporated creating the codons TTG (Leu) and TGT (Cys). If these two amino acids were not
429 found in other species then they would be non-extant. The cycling conditions for the PCR were
430 98°C for 30 s; 98°C for 20 s, 60 °C for 30s and 72°C for 1 min (25 cycles); and 72°C for 5 min.
431 The products were column-purified (QIAGEN, QIAquick PCR purification kit, 28104), eluted in
432 50 µl and mixed in equimolar proportion. The fusion-PCR was carried out by diluting 10 µl of
433 the mix to 25 µL of standard Phusion polymerase reaction mix in GC buffer. The cycling
434 conditions of the fusion-PCR were 98°C for 30 s; 98°C for 30 s, 60°C for 2 min and 72°C for 1
435 min (25 cycles); and 72°C for 5 min. The product of fusion was purified from agarose gel
436 (Qiagen, MinElute Gel Extraction Kit, 28604) and eluted in 10 µl of water. 10 µl of the product
437 was used as a template for additional 5 cycles of PCR reaction in Phusion polymerase reaction
438 mix (Thermo Fisher Scientific, F530S) in GC buffer, using primers 126 and 127. The cycling
439 conditions were as follows: 98°C for 30 s; 98°C for 20 s, 60°C for 30 s and 72°C for 1 min (5
440 cycles); and 72°C for 5 min. The product was column-purified (QIAGEN, QIAquick PCR
441 purification kit, 28104), and used as an insert for Gibson assembly.
442 To create a library of His3 mutants, pRS416 plasmid was amplified using primers 128
443 and 129. The insert was cloned into the vector using Gibson assembly (NEB, E2611S). Ligated
444 products (200 - 300 ng/µL) were desalted by drop dialysis using 13 mm diameter, Type-VS
445 Millipore membrane (Merck Millipore, VSWP01300). 20 µL ElectroMAX DH10B competent
446 cells (Invitrogen, 18290015) were electroporated with 3 µL ligated products. 0.01% of the
447 electroporated bacteria were plated on ampicillin-containing medium in order to estimate the
448 complexity of the library; the remaining culture was grown overnight in 100 ml of liquid
449 medium, and the plasmid was extracted the next day. For each library, the maximum number of
450 protein sequences that can be generated was computed. Libraries were generated until to total
451 complexity reached at least 3 times this value.
452
453 *Yeast transformation and yeast library generation*
454 For each segment, yeast strain LBCY47 (*his3*:KanMX*leu2*Δ0 *met15*Δ0 *ura3*Δ0, derived
455 from BY4741) was transformed with 50 µg of pRS416_His3 mutant library using lithium acetate
456 transformation and plated onto glucose synthetic complete dropout plates lacking uracil. After 40
457 hours' growth at 30°C, approximately 0.5 million yeast colonies were scraped off the plates,
458 mixed together and washed 2 times with 100 ml of PBS.
459
460 *Bulk competition*
461 $4x10^9$cells were inoculated into 500 ml of glucose synthetic complete dropout medium
462 lacking uracil with 200 mg/L of G418, and grown at 30°C at 220 RPM for 6-8 h in order to
463 eliminate clones with low fitness irrespective of histidine biosynthesis. Cells were later pelleted
464 and washed with 50 ml of PBS. Approximately 10^{10} cells were inoculated into 1 L of synthetic

465 complete dropout medium lacking histidine, and grown at 30°C at 220 RPM for 168 h with 12 h
466 between bottlenecks: ~10^{10} cells were transferred into fresh medium ~10^{8} cells from the culture
467 were kept as sample for the given time point. Bulk competition for each library of mutants was
468 done in two replicates to account for biological variability.
469
470 *NGS library preparation*
471 The relative abundance of yeast mutants was measured in 3 samples: 1) the initial
472 population before selection was applied (t0), 2) the population after 12 h of growth in the
473 selective medium (t1), and 3) the final population after 168 h of growth in the selective medium
474 (t14). In order to extract plasmid DNA, $5x10^{9}$ cells from each sample were incubated in 300 µL
475 of zymolyase buffer (1 M sorbitol, 0.1 M sodium acetate, 60mM EDTA (pH 7.0), 2 mg/ml
476 zymolyase, 1% 2-Mercaptoethanol) at 37°C for 3 h. The plasmid DNA was purified from the
477 obtained spheroplasts using QIAprep Spin Miniprep Kit (QIAGEN, 27104) according to the
478 manufacturer's protocol. The obtained DNA was used as a template in a 25 µL of Q5 DNA
479 polymerase reaction mix (NEB, M0491S), using staggered primers for demultiplexing in the
480 following cycling conditions: 98°C for 30s; 98°C for 10s, 60°C for 30s and 72°C for 30s (18
481 cycles); and 72°C for 2 min. PCR products were purified using Agencourt AM Pure XP beads
482 (Beckman Coulter, A63880), and eluted in 40 µL of TE buffer (pH 8.0). DNA extraction and
483 PCR-amplification were repeated twice for every sample to account for the technical variability.
484
485 NGS libraries were prepared from 100 ng of the purified DNA amplicons using Ovation Rapid
486 DR System (Nugen, 0319-32) according to manufacturer's instructions. Each library was
487 visualized on a Bioanalyzer (Agilent Technologies) and quantified by qPCR with a Kapa Library
488 Quantification Kit (Kapa Biosystems, KK4835). Twelve samples were pooled together
489 (accounting for two biological replicates, two technical replicates and three time points) at the
490 final concentration of 4 nM, and sequenced in the same lane. Samples were sequenced as 125-bp
491 paired-end reads on a HiSeq2500 sequencer (Illumina) with v4 sequencing chemistry.
492
493 *Yeast growth assay*
494 Mutant strains were grown overnight in complete dropout medium lacking uracil. The
495 cultures were diluted to 0.05 OD 600 nm, and grown for 5 h in the same medium. 6 µL of each
496 culture were transferred into 96-well plates in 125 µL of complete dropout medium lacking
497 histidine. Growth of the strains was monitored by measuring OD 600 nm every 10 min using
498 Tecan Infinite M1000 PRO microplate reader equipped with an integrated Stacker module.
499
500 The growth rate of individual curves was measured as the inverse of the time to grow
501 from OD = 0.135 = exp(-2) to OD = 0.368 = exp(-1). If the curve did not reach 0.368, the growth
502 was set to 0. Curves that crossed 0.135 or 0.368 were excluded. The growth rate of a clone was
503 measured as the median of 6 independent growth experiments. We excluded from the analysis
504 clones with discordance between growth in solid and liquid medium, clones that could not be
505 sequenced or that showed evidence of contamination by sequencing, and clones such that the
506 Kullback-Leibler divergence of their read counts compared to all synonymous clones was greater
507 than 0.22. The later criterion ensured that the selected clones were not outliers compared to other
508 variants encoding the same protein.
509
510 ***Growth rates of isolated strains***
511 We isolated 197 strains from all segment libraries of extant amino acid combinations (9-
512 26 strain per segment) and used Sanger sequencing to determine the sequence. For each strain
513 we performed 6 repeats of growth assay and calculated the average growth rate. Fitness values
514 from competition and growth rates are highly correlated ($r=0.82$ $p=10^{-48}$). Correlation was
515 significant and greater than 0.6 for all segments except S9, where all selected genotypes
516 appeared to be neutral (**Supplementary Fig. 3**).

517
518 ***Initial data filtering***
519 The individual sequences of the variants were recovered from pair-end reads with the
520 following steps: the constant region between the two variable regions was identified by inexact
521 matching allowing up to 20% errors using the Seeq library version 1.1.2
522 (https://github.com/ezorita/seeq). The reads are not oriented because the Illumina sequencing
523 adapters were added by ligation, so the constant regions were searched on both reads. Forward
524 and reverse reads were swapped when a match was found on the reverse read. This ensured that
525 all of the sequences are in the same orientation. For multiplexing purposes, the sample identity
526 was encoded in the left and right primers used to PCR-amplify the variants. To demultiplex the
527 reads, we used inexact matching with the candidate primers, allowing up to 20% errors. This
528 approach was faster and less error-prone than using FLASH[51]. To merge the reads, the sequence
529 of the reverse reads was reverse complemented and the constant region was searched by inexact
530 matching allowing up to 20% errors. The position of the constant part in each read indicated how
531 they must be stitched together. In the region of overlap, the consensus sequence was determined
532 by picking the nucleotide with highest quality as indicated in the quality line of the fastq files. If
533 'N' persisted in the final sequence, the reads were discarded. The PCR primers were trimmed so
534 that all the sequences of the same competition would start and end at the same location.
535 Reads that did not have the constant region, that could not be oriented or that could not
536 be demultiplexed were discarded. The remaining errors in the reads were corrected by sequence
537 clustering. We used starcode version 1.0 [ref. 52] with default parameters and allowing up to two
538 errors. The corrected reads were translated using the genetic code. Variants encoding the same
539 proteins were not merged; they were kept separate for downstream analyses. A running Docker
540 virtual machine with commented scripts to replay the whole the process is available for
541 download at https://hub.docker.com/r/gui11aume/epi/.
542
543 ***DNA sequence variant frequency calculation and data filtering***
544 The total number of reads for 12 segments, 3 time points and 4 replicas are shown in
545 **Supplementary Table 1**. Genotypes frequencies are defined as the number of reads for a given
546 genotype divided by the total number of reads in that replicate. Mean frequency was calculated
547 over 4 replicas to be used in further analysis. However, to eliminate influence of outliers the
548 median was taken instead of mean if absolute difference between mean and median was greater
549 than the median value. Only genotypes present in both technical replicas of both biological
550 replicas with at least ten reads (summed across all time points) in each of them were kept.
551
552 ***Noise estimation***
553 The major factors causing noise in genotype frequency measurements are sampling
554 errors, PCR amplification errors and genetic drift during the competition. For all of these factors,
555 the amount of error depends on the genotype frequency. Therefore, we estimated measurement
556 errors as the function of genotype frequency.
557 For a given segment, time point and a pair of biological or technical replicas for each
558 genotype we calculated the mean frequency and the squared difference of frequencies from these
559 two replicas. We sorted genotypes by mean frequency and grouped them such that each bin
560 contains 5000 genotypes. We calculated the average frequency and the average squared
561 difference in each bin. Additionally, squared error for frequency 0 was set equal to $\frac{1}{2}\cdot$
562 $\left(\left(\frac{0.5}{N_i}\right)^2+\left(\frac{0.5}{N_j}\right)^2\right)$, where N_i and N_j are total read numbers in replicas i and j. Finally, by linear
563 interpolation we obtained dependencies of squared differences as a function of frequency, $s_{ij}^2(f)$,
564 where i and j are different replicas.
565 Using squared differences from pairwise comparison of replicas we can estimate variance
566 of mean frequency over four replicas. Let numerate replicas 1, 2, 3, 4 where 1, 2 are technical

replicas of the first biological repeat and 3, 4 are the technical replicas of the second biological repeat. Errors coming from the competition (e.g.: genetic drift) are shared for replicas 1, 2 and for replicas 3, 4. Let's call them Δf_{b_1} and Δf_{b_2} and their variances $\sigma^2_{b_1}$ and $\sigma^2_{b_2}$ respectively. Technical errors of sampling from the population and from PCR are unique for each replica. Let's call them $\Delta f_{t_i}, i = 1..4$ and their variances $\sigma^2_{t_i}, i = 1..4$ respectively. All variances are function of frequency and writing $\sigma^2_{X_i}$ we assume $\sigma^2_{X_i}(f)$.

In the introduced notations the mean frequency over 4 replicas is:

$$f = \frac{1}{4} \cdot (f_1 + f_2 + f_3 + f_4) =$$

$$\frac{1}{4} \cdot \left(\left(f^* + \Delta f_{b_1} + \Delta f_{t_1}\right) + \left(f^* + \Delta f_{b_1} + \Delta f_{t_2}\right) + \left(f^* + \Delta f_{b_2} + \Delta f_{t_3}\right) + \left(f^* + \Delta f_{b_2} + \Delta f_{t_4}\right) \right) =$$

$$f^* + \tfrac{1}{2} \cdot \left(\Delta f_{b_1} + \Delta f_{b_2}\right) + \tfrac{1}{4} \cdot \left(\Delta f_{t_1} + \Delta f_{t_2} + \Delta f_{t_3} + \Delta f_{t_4}\right),$$

where f^* is the true frequency. Applying basic properties of variance the variance of mean frequency:

$$\sigma^2 = \frac{1}{4} \cdot \left(\sigma^2_{b_1} + \sigma^2_{b_2}\right) + \frac{1}{16} \cdot \left(\sigma^2_{t_1} + \sigma^2_{t_2} + \sigma^2_{t_3} + \sigma^2_{t_4}\right)$$

To estimate $\sigma^2_{b_1}, \sigma^2_{b_2}, \sigma^2_{t_1}, \sigma^2_{t_2}, \sigma^2_{t_3}, \sigma^2_{t_4}$ we used squared differences from pairwise comparison of replicas calculated above $s^2_{12}, s^2_{13}, s^2_{14}, s^2_{23}, s^2_{24}, s^2_{34}$:

$$\mathbb{E}[s^2_{12}] = \mathbb{E}[(\Delta f_{t_1} - \Delta f_{t_2})^2] = \sigma^2_{t_1} + \sigma^2_{t_2}$$
$$\mathbb{E}[s^2_{13}] = \mathbb{E}[(\Delta f_{b_1} + \Delta f_{t_1} - \Delta f_{b_2} - \Delta f_{t_3})^2] = \sigma^2_{b_1} + \sigma^2_{t_1} + \sigma^2_{b_2} + \sigma^2_{t_3}$$
$$\mathbb{E}[s^2_{14}] = \mathbb{E}[(\Delta f_{b_1} + \Delta f_{t_1} - \Delta f_{b_2} - \Delta f_{t_4})^2] = \sigma^2_{b_1} + \sigma^2_{t_1} + \sigma^2_{b_2} + \sigma^2_{t_4}$$
$$\mathbb{E}[s^2_{23}] = \mathbb{E}[(\Delta f_{b_1} + \Delta f_{t_2} - \Delta f_{b_2} - \Delta f_{t_3})^2] = \sigma^2_{b_1} + \sigma^2_{t_2} + \sigma^2_{b_2} + \sigma^2_{t_3}$$
$$\mathbb{E}[s^2_{24}] = \mathbb{E}[(\Delta f_{b_1} + \Delta f_{t_2} - \Delta f_{b_2} - \Delta f_{t_4})^2] = \sigma^2_{b_1} + \sigma^2_{t_2} + \sigma^2_{b_2} + \sigma^2_{t_4}$$
$$\mathbb{E}[s^2_{34}] = \mathbb{E}[(\Delta f_{t_3} - \Delta f_{t_4})^2] = \sigma^2_{t_3} + \sigma^2_{t_4}$$

Therefore, the variance of mean frequency f can be found as:

$$\sigma^2 = \frac{1}{16} \cdot \left((s^2_{13} + s^2_{14} + s^2_{23} + s^2_{24}) - (s^2_{12} + s^2_{34}) \right)$$

Recalling that variance and squared differences are a function of frequency:

$$\sigma^2(f) = \frac{1}{16} \cdot \left((s^2_{13}(f) + s^2_{14}(f) + s^2_{23}(f) + s^2_{24}(f)) - (s^2_{12}(f) + s^2_{34}(f)) \right)$$

For each segment and time point we calculated the numerical function $\sigma^2(f)$. Then for each genotype having mean frequency f_x we estimated its variance as $\sigma^2(f_x)$

Merging amino acid genotypes

We merged nucleotide genotypes that corresponded to the same amino acid sequence and summed their frequencies and variances. We filtered out all genotypes x which had any of following patterns:

$f_x^{t_0} = 0, f_x^{t_1} = 0, f_x^{t_2} > 0$ or $f_x^{t_0} = 0, f_x^{t_1} > 0, f_x^{t_2} = 0$ or $f_x^{t_0} > 0, f_x^{t_1} = 0, f_x^{t_2} > 0$. Fraction of such genotypes were <0.5% for all segments except S9, for which it was 4.5%

For further analysis, this amino acid dataset was used except when specified.

Fitness estimation

Number of cells in a pool with particular genotype x after time interval t increases exponentially

$$n_x^t = n_x^0 \cdot Exp[s_x \cdot t],$$

where s_x is absolute fitness. Frequency of genotype x as well depends exponentially on absolute fitness with an additional multiplicative factor:

$$f_x^t = \frac{n_x^t}{N^t} = \frac{n_x^0 \cdot Exp[s_x \cdot t]}{N^t} = \frac{f_x^0 \cdot Exp[s_x \cdot t]}{N^t/N^0},$$

where N^t and N^0 are total cell numbers in a pool at time points 0 and *t*. Factor $\frac{1}{N^t/N^0}$ reflects the total growth of population, it changes with time but is the same for all genotypes. Therefore, we can rewrite genotype frequency at time *t* as:

$$f_x^t = f_x^0 \cdot Exp[(s_x - \bar{s}^{0t}) \cdot t],$$

where $\bar{s}^{0t} = \frac{1}{t} \cdot Log\left(\frac{N^t}{N^0}\right)$

In the measured dataset for each genotype *x* we have 3 measurements of frequency $f_x^{t_0}$, $f_x^{t_1}$, $f_x^{t_2}$ and their errors $\sigma^2(f_x^{t_0}), \sigma^2(f_x^{t_1}), \sigma^2(f_x^{t_2})$. To estimate genotype fitness we minimized relative squared errors of exponential fit as function of fitness s_x and initial frequency f_x^0:

$$(s_x, f_x^0) = \mathrm{argmin}_{s_x, f_x^0}\left(\frac{\left(f_x^{t_0} - f_x^0\right)^2}{\sigma^2\left(f_x^{t_0}\right)} + \frac{\left(f_x^{t_1} - f_x^0 \cdot Exp[(s_x - \bar{s}^{01}) \cdot t_1]\right)^2}{\sigma^2(f_x^1)} + \frac{\left(f_x^{t_2} - f_x^0 \cdot Exp[(s_x - \bar{s}^{02}) \cdot t_2]\right)^2}{\sigma^2(f_x^2)}\right) \quad (1)$$

This formula contains four parameters common for all genotypes from one segment: $\bar{s}^{01}, \bar{s}^{02}, t_1, t_2$. Further we will perform additional shifting and scaling of fitness values (see next section), therefore, without loss of generality we could set $\bar{s}^{01} = 0$ and $t_1 = 1$. Ideally, t_2/t_1 should equal 14, however, we noticed that this ratio does not hold for many segments and fitted $k = t_2/t_1$ from data instead of using value 14.

To find specific $\bar{s}^{02}$ and k for each segment we selected genotypes with high frequencies at t_0 ($t_0 > 25 \cdot 10^{-6}$) which corresponds to ~500-1000 reads per technical replicate. Each segment contains 10^3-10^4 genotypes that meet this criterion. We minimized eq. (1) for selected genotypes trying all possible combinations of $(\bar{s}^{02}, k)$ from a grid where $\bar{s}^{02} \epsilon [0,1.2]$ with step 0.01 and $k \epsilon [1,14]$ with step 0.1 and choose $(\bar{s}^{02}, k)$ which gives minimal (*).

Finally, given $(\bar{s}^{02}, k)$ for each segment we found s_x for each genotype. Errors for fitness values, s_x^{std}, were estimated as standard error of best-fit parameter.

For genotypes with frequencies pattern $f_x^{t_0} > 0, f_x^{t_1} = 0, f_x^{t_2} = 0$ fit of eq. (1) cannot be obtained. Therefore we defined upper boundary for their fitness value as $s_x^{boundary} = Log\left(\frac{1}{\max(N_1^{t_1}, N_2^{t_1}, N_3^{t_1}, N_4^{t_1})}\right)$, where $N_i^{t_1}, i = 1..4$ are total read numbers at time point t_1 in *i* replica.

Fitness rescaling

We scaled fitness such that lethal genotypes have fitness 0 and neutral genotypes have fitness 1. We assumed that genotypes with a stop codon or frame shift are lethal. Thus, for each segment we linearly rescaled the fitness distribution so that 95% of genotypes with nonsense mutations have a fitness of 0 and so that the local maximum of the fitness distribution of genotypes with extant amino acids is 1. The scaling around the local maximum led to the shift of fitness values of less than +/- 0.025 in each of the 12 segments compared to the measured wildtype strains and did not affect our results (for scale, we called a substitution non-neutral if its effect on fitness was > 0.4). All fitness values which became smaller than 0 were set to 0.

Quality control and comparison of synonymous sequences

We used nucleotide synonymous sequences as an internal control. The error rate for a measurement of fitness of an amino acid sequence depends on the number of synonymous sequences, *n*, that were used to estimate it. Therefore, we estimated the false discovery rates separately for categories with *n=1,..10* variants. For each amino acid genotype with more than *n*

synonymous variants we merged random combination of *n* of its nucleotide genotypes and estimated fitness. We then calculated the difference between this fitness and the fitness of the corresponding amino acid sequence. We classified case as "false unfit" if difference was <-0.4 and as "false fit" if difference was >0.4. The fraction of such cases gives us false discovery rates for genotypes having *n* synonymous variants. To get total false discovery rates for each segment we averaged "false unfit" and "false fit" rates for different *n* with weights equal to the fractions of genotypes in amino acid dataset which have *n* synonymous variant (**Supplementary Table 1**). The high correlation between biological replicas (**Supplementary Table 6**) confirms high accuracy of our high-throughput experiments, with the exception of segment 9.

Predicting fitness using deep learning

To predict the unidimensional fitness function based on additive contribution of extant amino acid states we used deep learning, a powerful machine learning technique, capable of constructing virtually any function, even with a simple neural network architecture. To convert amino acid sequences into a binary feature matrix we used one-hot encoding strategy, in which each feature (column in the matrix) indicates the presence or absence of a particular amino acid state.

To optimise the accuracy/overfitting ratio, we tested over a hundred of different neural network architectures and parameters. As a starting point, we selected a number of complicated architectures, which describe our data, but are prone to overfitting due to a large number of parameters. We then gradually reduced the number of layers and neurons to reduce the overfitting, while controlling for accuracy.

Our final architecture consists of three layers and 22 neurons in total (**Supplementary Fig. 4**). Each of the neurons performs a linear transformation of the input and subsequently applies a non-linear activation function (a sigmoid) to the result. The output of the first layer, therefore, is a sigmoid of a linear transformation of the feature vector ($c_1^T x$). The second layer decompresses the hidden nonlinear representation into 20 sigmoids, the combination of which is further linearly transformed with the only neuron of the third layer and wrapped into another sigmoid function:

$$F(x) = \sigma\left(\sum_{i=1}^{20} c_{3,i}\,\sigma\left(c_{2,i}\,\sigma\left(c_1^T x + b_1\right) + b_{2,i}\right)\right)$$

where $\sigma(t) = \frac{1}{(1+exp(-t))}$, x – is the feature vector, $\boldsymbol{c}_1$ – the vector of coefficients, corresponding to the first layer, $c_{n,k}$ - coefficient corresponding to the *n*-th layer and the *k*-th neuron, b_n - bias corresponding to the *n*-th layer. Crucially, this relatively simple architecture is capable of fitting virtually any function[53], thus, in contrast to conventional logistic regression, in our approach we select the correct model from a vast variety of functions.

The key idea of our approach is that the number of neurons in the first layer of the neural network determines the number of linear combinations of mutations (or fitness potentials) used in order to predict mutant fitness. In other words, each neuron in the first layer assigns a single unique weight to every amino acid state in the dataset (**Supplementary Fig. 4**). Multiplication of such weight vectors and binary genotype vectors result in fitness potential. Thus, the number of neurons in the first layer of the architecture basically determines the dimensionality of epistasis we assume. The obtained fitness potentials are then transformed by a nonlinear phase shift function constructed by the 22 neurons of the neural network.

The architecture simplicity avoids overfitting, which was further prevented by using early stopping and keeping 10% of data as a test set. The loss function that is being optimised in our experiments is not convex, which leads to a high probability of getting stuck in different local minima. To ensure reproducibility, each of our models was constructed ten independent times using random train-test splits.

Each model was trained for under 100 epochs using mean squared error as the loss function. An unpublished adaptive learning rate method proposed by Geoff Hinton, RMSProp, was used as the optimiser. This algorithm is a version of a mini-batch stochastic gradient descent, utilising the gradient magnitude of the recent gradients in order to normalise the current ones. All the weights were initialised using Xavier normal initialiser[54].

Paths between pairs of fit genotypes

For analysis in **Fig. 6d**, we first choose two fit "parental" genotypes, one randomly chosen genotype (eg: ABE) and the other parental genotype that is either *S. cerevisiae* wildtype genotype (inter-segmental) or another random fit genotype in the data (intra-segmental) (eg: abe). The two genotypes in this example are Hamming Distance 3 apart (HD=3). We next compute all (HD2-2) intermediate genotypes (eg: AbC, aBc, *et cetera*) and retain the subset that were experimentally measured. We represent the two parental genotypes and all measured intermediate genotypes as an undirected graph in which each genotype is a vertex. All genotypes one substitution apart are connected by an unweighted edge. The shortest possible path for a given pair of genotypes is of length HD. We find all shortest paths between the two parental genotypes using a breadth-first search. We next remove all vertices (genotypes) that are unfit, and recompute the number of shortest between the two parental genotypes. For example, in **Fig. 6a**, there are six paths of length three if you take into account all genotypes, but only three paths of length three if you take into account only fit genotypes.

Clustering of unfit genotypes in sequence space

For the analysis in **Fig. 6e**, we first represent the two parental genotypes and all measured intermediate genotypes as an undirected graph in which each genotype is a vertex. All genotypes one substitution apart are connected by an unweighted edge. We can then compute the degree (number of genotypes of distance one) for each vertex (genotype). We do so randomly drawing from all measured genotypes and using only unfit genotypes or using the same number but randomly chosen genotypes. For the randomly chosen genotypes, the value is the average over 1000 runs.

Quantifying sign epistasis

For each substitution (eg: C -> S at position 141), we considered only those that exhibit a large fitness effect (abs. difference > 0.4) comprising a set of substitutions with large effects. For each substitution we divided the genetic backgrounds into two categories: those in which the substitution caused a > 0.4 increase in fitness, and those backgrounds in which the substitution caused > 0.4 decrease in fitness. A single substitution can cause a large increase in fitness in some backgrounds and a large decrease in others due to two possible reasons: sign epistasis or experimental error. To differentiate the two cases, we identified secondary substitutions that significantly alter the ratio of large increases to large decreases in fitness (Fisher's exact test, Bonferroni corrected p-value < 0.05). We only consider a site to be under sign epistasis if there is a second site that alters the frequency of sign epistasis in a statistically significant manner, i.e. more frequently than expected by chance alone.

Structural analysis

Structure prediction

An initial model was obtained with the I-TASSER server[55]. The list of top 10 PDB structural templates picked up by the I-TASSER included high-quality crystal structures of imidazoleglycerol-phosphate dehydratases from *Arabidopsis thaliana* and *Cryptococcus neoformans.* Coordinates of the top-scoring model (C-score=0.21, estimated TM-score = 0.74±0.11, estimated RMSD = 5.1±3.3Å) and the predicted normalized B-factor[56] were used for further analysis. The value of the model quality metric (TM-score >0.5) indicates a model of

correct topology. The proteins structurally close to the final model (RMSD 0.6 - 1.7Å are PDB IDs 4MU0, 4GQU, 1RHY, 5DNL and 2AE8 from *Arabidopsis thaliana*, *Mycobacterium tuberculosis*, *Cryptococcus neoformans*, *Pyrococcus furiosus* and *Staphylococcus aureus*.

We measured the distribution of distances (in angstroms) between pairs of residues that exhibit strong sign epistasis (**Supplementary Table 1**, ReallyPositivePair == TRUE), and compared it with the distribution of pairwise distances among residues for which we have sufficient data to be certain that a given pair does not exhibit sign epistasis (**Supplementary Table 1**, ReallyNegativePair == TRUE).

ΔΔG prediction

Cartesian_ddg application[57] from Rosetta version 2017.08.59291 was used for ΔΔG predictions. Top-scoring I-TASSER model was pre-minimized using the Relax[58] application in dual-space[59] with the flags: -relax:dualspace true; -ex1; -ex2; -use_input_sc; -flip_HNQ; -no_optH false; -relax:min_typelbfgs_armijo_nonmonotone; -nonideal. The best scoring model from 1000 structures was selected. The effect of up to 4 mutations (54,500 genotypes in total) was assessed in Cartesian space with the Talaris_2014 score function, and the -fa_max_dis 9.0 flag. ΔΔG was estimated as a difference of mean score for 3 independent runs for every mutant and the wild-type score.

766
767 **Figures**
768
769 **Figure 1. Combinatorial approach to the study of fitness landscapes.** A fitness landscape is
770 the representation of fitness for all possible genotypes composed of a specific set of loci. **a,**
771 Following Figure 1 from Sewall Wright ref. [6] consider the genotype space consisting of 5 loci,
772 each with two allele states (lower and uppercase letters). The entire genotype space is 5-
773 dimensional consisting of 2^5 genotypes. Given two genotypes found in extant species (abCde and
774 ABCdE in this example), surveying combinations of extant alleles substantially reduces the
775 dimensionality of the genotype space, concomitantly reducing the number of genotypes to assay.
776 The surveyed area (blue cube) considers all combinations of allele substitutions that have
777 occurred in the course of evolution between the two sequences (red line), avoiding the sampling
778 of combinations with less relevance to the evolutionary trajectory (black lines). **b,** Given the
779 entire multidimensional genotype space (black circle) our approach considers an
780 multidimensional subspace consisting of the combinatorial set of amino acid states from extant
781 species. The blue line represents the yeast phylogeny and the surrounding blue space represents a
782 multidimensional set of combinations of extant amino acids of the sequence under consideration,
783 one His3 gene segment in our study. By contrast, random mutagenesis studies consider only a
784 local segment of the genotype space surrounding a specific genotype (green circle). **c**, A multiple
785 alignment of orthologous sequences of His3 for segment 2 for which we incorporated almost all
786 extant amino acid states from 21 yeast species (blue bars) and 10-100% extant states from a set
787 of 396 orthologues (grey bars). **d**, The predicted structure of His3p with amino acid residues that
788 were substituted in our library.
789
790 **Figure 2. Visual representations of the fitness landscape. a,** The fitness landscape for all
791 assayed genotypes in segment 7. Nodes represent unique amino acid sequences with edges
792 connecting those separated by a single amino acid substitution. Colour saturation represents the
793 minimum fitness of the two connected nodes. **b,** For segment 7, fitness of ancestral and extant
794 nodes and genotypes one substitution away from the nodes in the background of *S. cerevisiae*
795 gene on the yeast phylogeny (black lines), are shown in colour ranging from grey (lowest fitness)
796 to blue (highest fitness).
797

Figure 3. Fitness distributions. a, The distribution of fitness for genotypes composed of combination of extant amino acid states (green) and non-extant amino acid states (purple) at the same positions. **b**, The fraction of unfit genotypes per segment among genotypes consisting entirely from extant amino acid states (green) and those incorporating non-extant amino acid states (purple). **c**, The number of genotypes with high fitness that incorporates specific amino acid states. For each amino acid state, the number of genetic backgrounds that contain that amino acid state and are fit (fitness > 0) are shown. **d**, The percent of backgrounds in which a specific substitution is neutral (white), beneficial (blue) or deleterious (grey). The region marked in green shows substitutions that never have large effects (> 0.4) on fitness. Beneficial and deleterious effects are shown only if the frequency for a given substitution was higher than the false discovery rate (**Supplementary Table 1**). Data from segment 9 were excluded for this figure.

Figure 4. Epistasis and the His3 fitness landscape for segments 2, 5 and 7. **a**, Fitness as a function of a single fitness potential (black curve, the fitness of individual genotypes is orange). **b**, A network depiction of sign epistasis between amino acid substitutions. Colour coded sites with reciprocal sign epistasis (black lines) and unidirectional interactions (grey arrows) are shown. **c**, Genotypes containing substitutions with a higher number of sign epistatic interactions are less likely to be fit by the threshold function of the fitness potential. **d**, Increasing the number of neurons in the first layers of the neural network, which is equivalent to increasing the number of underlying fitness potentials, leads to more accurate models for segments with detected sign epistasis. Each dot corresponds to an independent optimization of model parameters. **e**, Fitness as a function of two fitness potentials (black dots, measured fitness is depicted in orange).

Figure 5. Sign epistasis. a, Substitution C->S at site 141 in segment 2 more frequently has a positive effect on fitness in the background of T at site 143, a negative effect in the background of 143I and is equally likely to be strongly deleterious or strongly beneficial in the background of 143V. **b**, Predicted change in free energy following a C141S substitution in all genetic backgrounds with an I or T at 143 and that are closer than four mutations away from *S. cerevisiae*. **c**, Distribution of the number of substitutions at each site under sign (yellow) and reciprocal sign (orange) epistasis. Sites with 0 interactions do not exhibit sign epistasis. **d**, The fraction of genotypes in which the substitution under sign epistasis has the less frequent effect on fitness.

Figure 6. Analysis of evolutionary pathway accessibility. a, A threshold fitness potential function can lead to some paths being inaccessible between two genotypes of high fitness (abe, ABE) if the joint contribution of several alleles to the fitness potential (abE, aBE) leads to the fitness potential below the threshold. **b,** The fraction of unfit intermediate genotypes between two fit genotypes as a function of their average fitness potential. **c**, The grey area represents all genotypes in segment 7. When two fit genotypes (red dots) have high fitness potential, many paths between them will be accessible because many intermediate genotypes will also have high fitness potential and fitness (blue dots). **d**, The fraction of accessible shortest paths between two fit genotypes with unfit genotypes from data (orange) or the same number of randomly selected genotypes (grey), shown as a function of Hamming distance between two fit genotypes. Error bars are standard deviation. **e**, On a graph with genotypes connected by edges if they are one substitution apart we calculate the degree of connectivity (number of edges for each node) for all genotypes (blue), only unfit (fitness = 0) genotypes (orange) and a graph with the same number of nodes as the graph with unfit genotypes but with nodes chosen at random (grey).

854
855 **Supplementary Figures**
856
857 **Supplementary Figure 1. Experimental design. a,** The sequence of the His3 protein from S.
858 cerevisiae was separated into 12 independent segments of similar lengths, such that the full
859 combinatorial set of extant amino acid substitutions was less than 100,000 possible genotypes.
860 These segments represented different combinations of structural elements of the His3 protein
861 structure. **b,** For each of the 12 segments from His3, we selected extant amino acid states using a
862 multiple alignment of His3 orthologues from 396 species, preferentially incorporating states
863 from 21 yeast species, the variability is shown in segment 3 as an example. Mutant degenerate
864 codon libraries were constructed by fusion PCR of two synthesized variable halves of each
865 segment. These high-complexity plasmid libraries were transformed into haploid His3 knockout
866 S. cerevisiae strain. The growth rate of yeast carrying different extant amino acid state
867 combinations in His3 gene was measured using serial batch culture in the absence of histidine
868 with 12 hours between ~100-fold dilutions. To estimate the fitness of yeast mutants their relative
869 abundance was measured at three points: in the initial population before selection (t0), in the
870 population after 12 hours of growth in the selective medium (t1), and in the final population after
871 168 hours of growth in the selective medium (t14). To assess the fitness of individual mutants
872 the segments from three populations were amplified and sequenced. The relative abundance of
873 each sequence was used as a proxy for abundance of the associated yeast mutant, which in turn
874 determines its fitness. **c**, Secondary structure of His3 mapped to the segments in our
875 experiments.
876
877 **Supplementary Figure 2. Segment-specific fitness distributions for extant and non-extant**
878 **amino acid states. a,** The fitness distribution for each segment for genotypes consisting only of
879 extant amino acid states (green) or that contain one or more non-extant amino acid states
880 (purple) only at positions with a substitution in the extant library. **b,** The fitness distribution for
881 each segment for genotypes consisting only of extant amino acid states (green) and genotypes
882 with mutations at other positions in that segment (red).
883
884 **Supplementary Figure 3. Growth rate measurement of isolated strains. a,** Comparison of
885 fitness values from the pooled competition assay with growth rates of isolated strains as
886 measured in a microplate reader. Error bars for growth rates show s.e.m. of 6 replicates. **b**,
887 Pearson correlation coefficients between fitness values from competition and growth rates of
888 isolated strains for each segment. ** signifies p-value < 0.005 (correlation test). **c**, His3p
889 orthologues from different species complement a Δ his3 deletion in *S. cerevisiae*. Growth rates
890 of transformants containing whole HIS3 orthologous genes from other yeast species. Error bars
891 for growth rates show s.e.m. of ≥ 7 replicates.
892
893 **Supplementary Figure 4. Schematic representation of the deep learning approach.** Each
894 genotype was encoded as a binary vector (x). During training, each of the substitutions was
895 assigned a coefficient (c_i), comprising a vector of coefficients (c). The multiplication of these
896 two vectors is the fitness potential of the genotype. After going through three layers, each with a
897 sigmoid activation function, the predicted fitness is obtained.
898
899 **Supplementary Figure 5. The fitness potential of the His3 fitness landscape. a**, Fitness
900 potential predicted by the neural network as a function of the measured fitness for all 12
901 segments. **b**, The correlation between the fitness predicted by the fitness potential and the
902 measured fitness. **c,** Training and test R^2 for each segment for 20-fold cross-validation.
903
904

Supplementary Figure 6. Sign epistasis dimensionality graphs for all twelve segments. Each node represents a substitution, with multiple substitutions at the same site having the same colour. Substitutions under reciprocal sign epistasis are indicated by black lines while grey arrows indicate unidirectional sign epistasis.

Supplementary Figure 7. Multidimensional description of epistasis in His3 segments. a, Increasing the number of neurons in the first layer of the neural network, which is equivalent to increasing the number of underlying fitness potentials, leads to more accurate models for segments with detected sign epistasis. Each dot corresponds to an independent optimization of model parameters. **b,** Number of sign epistatic interactions of certain substitutions against average model prediction power for mutants including these substitutions.

Supplementary Figure 8. Protein stability and the fitness potential. a, A comparison of correlation coefficients between predicted and measured values across segments. **b,c**, correlations between the estimated impact of substitutions on free energy ($\Delta\Delta G$), fitness potential and fitness. $\Delta\Delta G$ correlates better with fitness potential than with fitness. **d**, Pairs of sites that exhibit sign (connected by a light edge in Supplementary Figure 6) and those that exhibit reciprocal sign epistasis (connected by a dark edge in Supplementary Figure 6) are closer together in the His3p structure that randomly chosen non-connected pairs of positions that exhibit sign epistasis.

Supplementary Figure 9. Decoupling inter- and intra-segmental epistasis. a, The fraction of unfit genotypes between *S. cerevisiae* and any other genotype consisting of extant amino acid states with high (blue) or any (red) fitness, and genotypes in the latter but not the former category (black) as a function of the Hamming distance between the two boundary genotypes. Points indicate median, the bars and lines indicate 50% of the genotypes and genotypes 2.7 sigmas from the mean, respectively. **b,** The neural network model assigns higher weights to amino acid states that that first occur in His3 orthologues farther from *S cerevisiae,* indicating the presence of intrasegmental interactions.

Supplementary Information 1. Multiple alignment of His3 orthologues.

Supplementary Information 2. Multidimensional description of epistasis in His3 segments. Fitness as a function of two fitness potentials (black dots, measured fitness is depicted in orange).

References

1. Dean, A. M. & Thornton, J. W. Mechanistic approaches to the study of evolution: the functional synthesis. *Nature Rev. Genet.* **8**, 675–688 (2007).

2. Kogenaru, M., de Vos, M. G. J., & Tans, S. J. Revealing evolutionary pathways by fitness landscape reconstruction. *Crit. Rev. Biochem. Mol. Biol.* **44**, 169–174 (2009).

3.Mackay, T. F. C. Epistasis and quantitative traits: using model organisms to study gene-gene interactions. *Nature Rev. Genet.* **15**, 22–33 (2014).

4. de Visser, J. A. G. M. & Krug, J. Empirical fitness landscapes and the predictability of evolution. *Nature Rev. Genet.* **15**, 480–490 (2014).

5. de Visser, J. A. G. M., Cooper, T. F., & Elena, S. F. The causes of epistasis. *Proc. Biol. Sci.* **278**, 3617–3624 (2011).

6. Wright, S. The roles of mutation, inbreeding, crossbreeding and selection in evolution. *Proc. Sixth Int. Congr. Genet.* **1**, 356–366 (1932).

7. Olson, C. A., Wu, N. C. & Sun, R. A comprehensive biophysical description of pairwise epistasis throughout an entire protein domain. *Curr. Biol.* **24**, 2643–2651 (2014).

8. Puchta, O., Cseke, B., Czaja, H., Tollervey, D., Sanguinetti, G., and Kudla, G. Network of epistatic interactions within a yeast snoRNA. *Science*. **352**, 840–844 (2016).

9. Li, C. Qian, W. Maclean, C. J. & Zhang, J. The fitness landscape of a tRNA gene. *Science* **352**, 837–840 (2016).

10. Sarkisyan, K.S., et al. Local fitness landscape of the green fluorescent protein. *Nature* **533**, 397–401 (2016.)

11. Hietpas, R. T., Bank, C., Jensen, J. D. & Bolon, D. N. A. Shifting fitness landscapes in response to altered environments. *Evolution* **67**, 3512–3522 (2013).

12. Parera, M. & Martinez, M. A. Strong epistatic interactions within a single protein. *Mol. Biol. Evol.* **31**, 1546–1553 (2014).

13. Podgornaia, A. I. & Laub, M. T. Pervasive degeneracy and epistasis in a protein-protein interface. *Science* **347**, 673–677 (2015).

14. Anderson, D. W. McKeown, A. N. & Thornton, J. W. Intermolecular epistasis shaped the function and evolution of an ancient transcription factor and its DNA binding sites. *Elife* **4**, e07864 (2015).

15. Meini, M. R., Tomatis, P. E., Weinreich, D. M. & Vila, A. J. Quantitative description of a protein fitness landscape based on molecular features. *Mol. Biol. Evol*. **32**, 1774–1787 (2015).

16. Bank, C., Matuszewski, S., Hietpas, R. T. & Jensen, J. D. On the (un)predictability of a large intragenic fitness landscape. *Proc. Natl. Acad. Sci. USA*. 113, 14085–14090 (2016).

17. Poelwijk, F.J., Kiviet, D.J., Weinreich, D.M., & Tans, S.J. Empirical fitness landscapes reveal accessible evolutionary paths. *Nature* **445**, 383–386(2007).

18. Gong, L. I. Suchard, M. A.& Bloom, J.D. Stability-mediated epistasis constrains the evolution of an influenza protein. *Elife* **2**, e00631(2013).

19. Gong, L. I.& Bloom, J.D. Epistatically interacting substitutions are enriched during adaptive protein evolution. *PLoS Genet.* **10**, e1004328(2014).

20. Starr, T. N. & Thornton, J. W. Epistasis in protein evolution. *Protein Sci.* **25**, 1204–1218 (2016).

21. Kumar, A. Natarajan, C. Moriyama, H. Witt, C.C. Weber, R.E. Fago, A.& Storz, J.F. Stability-mediated epistasis restricts accessible mutational pathways in the functional evolution of avian hemoglobin. *Mol. Biol. Evol.* **34**, 1240–1251(2017).

22. Tufts, D. M., *et al.* Epistasis constrains mutational pathways of hemoglobin adaptation in high-altitude pikas. *Mol. Biol. Evol.* **32**, 287–298 (2015).

23. Eyre-Walker A. & Keightley P. D. The distribution of fitness effects of new mutations. *Nat. Rev. Genet.* 8, 610–618 (2007).

24. Draghi, J. A. & Plotkin, J. B. Selection biases the prevalence and type of epistasis along adaptive trajectories. *Evolution* **67**, 3120–3131 (2013).

25. Lunzer, M., Miller, S. P., Felsheim, R. & Dean, A. M. The biochemical architecture of an ancient adaptive landscape. *Science* **310**, 499–501 (2005).

26. Palmer, A. C., Toprak, E., Baym, M., Kim, S., Veres, A., Bershtein, S. & Kishony, R. Delayed commitment to evolutionary fate in antibiotic resistance fitness landscapes. *Nat. Commun*. **6**, 7385 (2015).

27. Lalić, J. & Elena, S. F. Magnitude and sign epistasis among deleterious mutations in a positive-sense plant RNA virus. *Heredity* **109**, 71–77 (2012).

28. Keefe, A. D. & Szostak, J. W. Functional proteins from a random-sequence library. *Nature* **410**, 715–718 (2001).

29. du Plessis, L. Leventhal, G.E. & Bonhoeffer, S. How good are statistical models at approximating complex fitness landscapes? *Mol. Biol. Evol.* **33**, 2454–2468(2016).

30. Lum, P. Y. Edwards, S.& Wright, R. Molecular, functional and evolutionary characterization of the gene encoding HMG-CoA reductase in the fission yeast, *Schizosaccharomyces pombe*. *Yeast* **12**, 1107–1124 (1996).

31. Kondrashov, A.S. Sunyaev, S. & Kondrashov, F. A. Dobzhansky-Muller incompatibilities in protein evolution. *Proc. Natl. Acad. Sci. USA* **99**, 14878–14883 (2002).

1045 32. Kvitek, D. J. & Sherlock, G. Reciprocal sign epistasis between frequently experimentally
1046 evolved adaptive mutations causes a rugged fitness landscape. *PLoS Genet.***7**, e1002056 (2011).
1047
1048 33. Breen, M. S., Kemena, C., Vlasov, P. K., Notredame, C. & Kondrashov, F. A. Epistasis as
1049 the primary factor in molecular evolution. *Nature* **490**, 535–538 (2012).
1050
1051 34. Gavrilets, S. Evolution and speciation on holey adaptive landscapes. *Trends Ecol. Evol.* **12**,
1052 307–312(1997).
1053
1054 35. Salverda, M. L. M., Dellus, E., Gorter, F. A., Debets, A.J. M., van der Oost, J. Hoekstra, R.
1055 F. Tawfik, D. S. & de Visser, J.A.G. M. Initial mutations direct alternative pathways of protein
1056 evolution. *PLoS Genet.* **7**, e1001321(2011).
1057
1058 36. Weinreich, D. M., Delaney, N. F., de Pristo, M. A. & Hartl, D.L. Darwinian evolution can
1059 follow only very few mutational paths to fitter proteins. *Science* **312**, 111–114(2006).
1060
1061 37. Milkman, R. Selection differentials and selection coefficients. *Genetics* **88**, 391–403 (1978).
1062
1063 38. Kimura, M. & Crow J. F. Effect of overall phenotypic selection on genetic change at
1064 individual loci. *Proc. Natl. Acad. Sci. USA*. **75**, 6168–6171 (1978).
1065
1066 39. Kondrashov, F. A. & Kondrashov, A. S. Multidimensional epistasis and the disadvantage of
1067 sex. *Proc. Natl. Acad. Sci. USA*. **98**, 12089–12092 (2001).
1068
1069 40. Crow, J. F. & Kimura, M. Efficiency of truncation selection. *Proc. Natl. Acad. Sci. USA* **76**, 396–
1070 399 (1979).
1071
1072 41. Weinreich, D. M. Lan, Y. Wylie, C. S.& Heckendorn, R. B. Should evolutionary geneticists
1073 worry about higher-order epistasis? *Curr. Opin. Genet. Dev.* **23**, 700–707 (2013).
1074
1075 42. Poelwijk, F.J. Krishna, V. & Ranganathan, R. The Context-Dependence of Mutations: A
1076 Linkage of Formalisms. *PLoS Comput. Biol.* **12**, e1004771 (2016).
1077
1078 43. Sailer, Z. R. & Harms, M. J. High-order epistasis shapes evolutionary trajectories. *PLoS*
1079 *Comput. Biol.* **13**, e1005541 (2017).
1080
1081 44. Weinreich, D. M. Watson, R. A. & Chao, L. Perspective: Sign epistasis and genetic
1082 constraint on evolutionary trajectories. *Evolution* **59**, 1165–1174 (2005).

1083 45. Rokyta, D. R. et al. Epistasis between beneficial mutations and the phenotype-to-fitness Map
1084 for a ssDNA virus. *PLoS Genet*. **7**, e1002075 (2011).
1085
1086 46. Kondrashov, D. A. & Kondrashov, F. A. Topological features of rugged fitness landscapes in
1087 sequence space. *Trends Genet*. **31**, 24–33 (2015).
1088
1089 47. De Pristo, M. A. Weinreich, D. M. & Hartl, D. L. Missense meanderings in sequence space:
1090 a biophysical view of protein evolution. *Nature Rev. Genet.* **6**, 678–687 (2005).

1091 48. Bershtein, S., Segal, M., Bekerman, R., Tokuriki, N. & Tawfik, D. S. Robustness epistasis
1092 link shapes the fitness landscape of a randomly drifting protein. *Nature* **444**, 929–932 (2006).

1093 49. Orr, H. A. The population genetics of speciation: the evolution of hybrid incompatibilities.
1094 *Genetics* **139**, 1805–1813 (1995).

1095 50. Tamura, K., Stecher, G., Peterson, D., Filipski, A. & Kumar, S. MEGA6: Molecular
1096 Evolutionary Genetics Analysis version 6.0. *Mol Biol Evol*. **30**, 2725–2729 (2013).

1097 51. Magoč, T. & Salzberg, S. L. FLASH: fast length adjustment of short reads to improve
1098 genome assemblies. *Bioinformatics* **27**, 2957–2963 (2011).

1099 52. Zorita, E., Cuscó, P. & Filion, G. J. Starcode: sequence clustering based on all-pairs search.
1100 *Bioinformatics* **31**, 1913–1919 (2015).

1101 53. LeCun, Y., Bengio, Y. & Hinton, G. Deep learning. *Nature*. **521**, 436–444 (2015).

1102 54. Glorot, X. & Bengio, Y. Understanding the difficulty of training deep feedforward neural
1103 networks. In Proceedings of the 13th International Conference on Artificial Intelligence and
1104 Statistics (2010).
1105
1106 55. Yang, J. & Zhang, Y. I-TASSER server: new development for protein structure and function
1107 predictions. *Nucleic Acids Res.* **43**, W174–W181(2015).

1108 56. Yang, J., Wang, Y. & Zhang, Y. ResQ: An Approach to Unified Estimation of B-Factor and
1109 Residue-Specific Error in Protein Structure Prediction. *J. Mol. Biol.* **428,** 693–701 (2016).
1110
1111 57. Park, H., Bradley, P., Greisen, P. Jr., Liu, Y., Mulligan, V. K., Kim, D.E., Baker, D. &
1112 DiMaio, F. Simultaneous optimization of biomolecular energy functions on features from small
1113 molecules and macromolecules. *J. Chem. Theory Comput.* **12**, 6201–6212 (2016).

1114 58. Nivón, L. G., Moretti, R. & Baker, D. A Pareto-optimal refinement method for protein
1115 design scaffolds. *PLoS One* **8**, e59004 (2013).

1116 59. Conway, P., Tyka, M. D., DiMaio, F., Konerding, D. E. & Baker, D. Relaxation of backbone
1117 bond geometry improves protein energy landscape modeling. *Protein Sci.* **23**, 47–55 (2014).

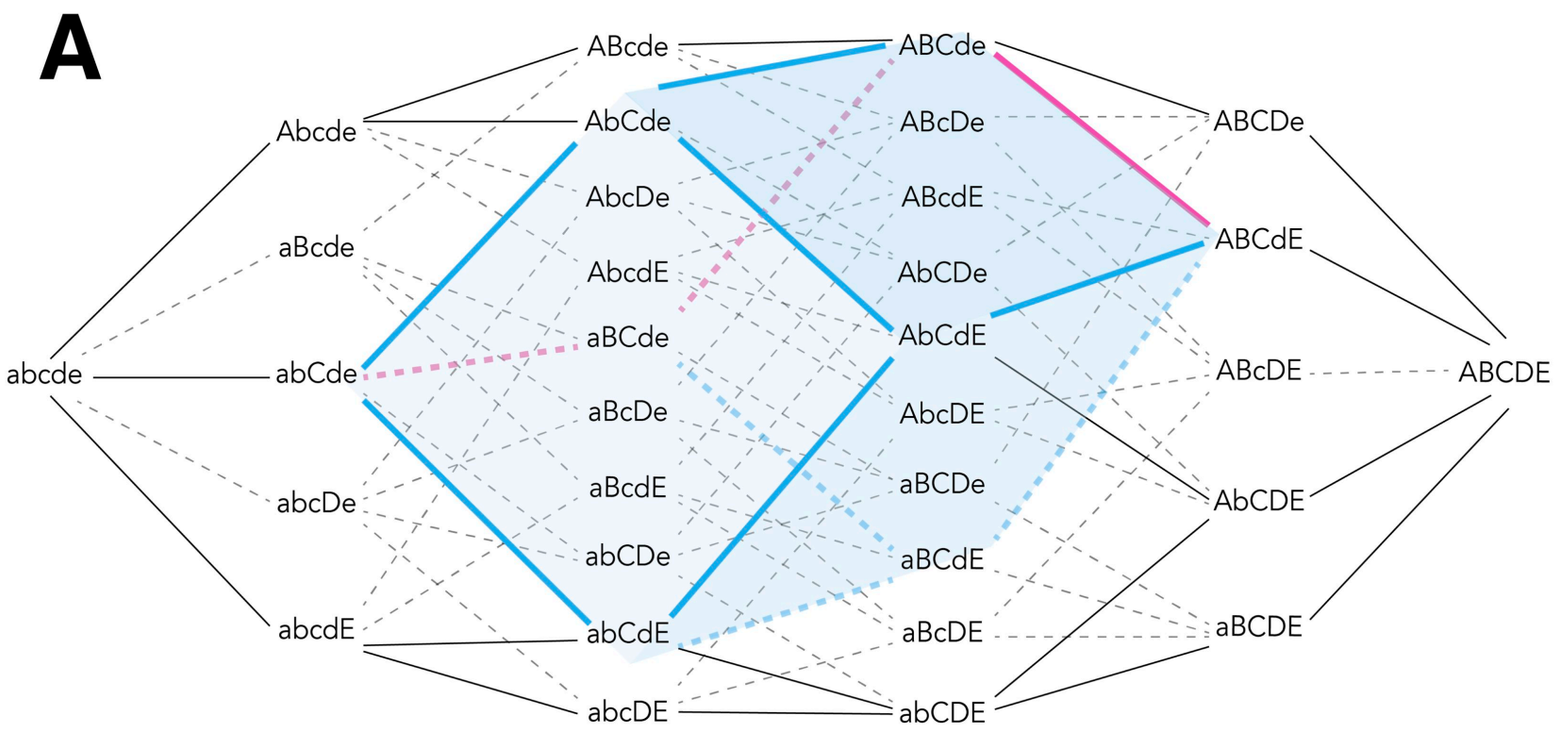
A
abcde
Abcde
aBcde
abCde
abcDe
abcdE
ABcde
AbCde
AbcDe
AbcdE
aBCde
aBcDe
aBcdE
abCDe
abCdE
abcDE
ABCde
ABcDe
ABcdE
AbCDe
AbCdE
AbcDE
aBCDe
aBCdE
aBcDE
abCDE
ABCDe
ABCdE
ABcDE
AbCDE
aBCDE
ABCDE

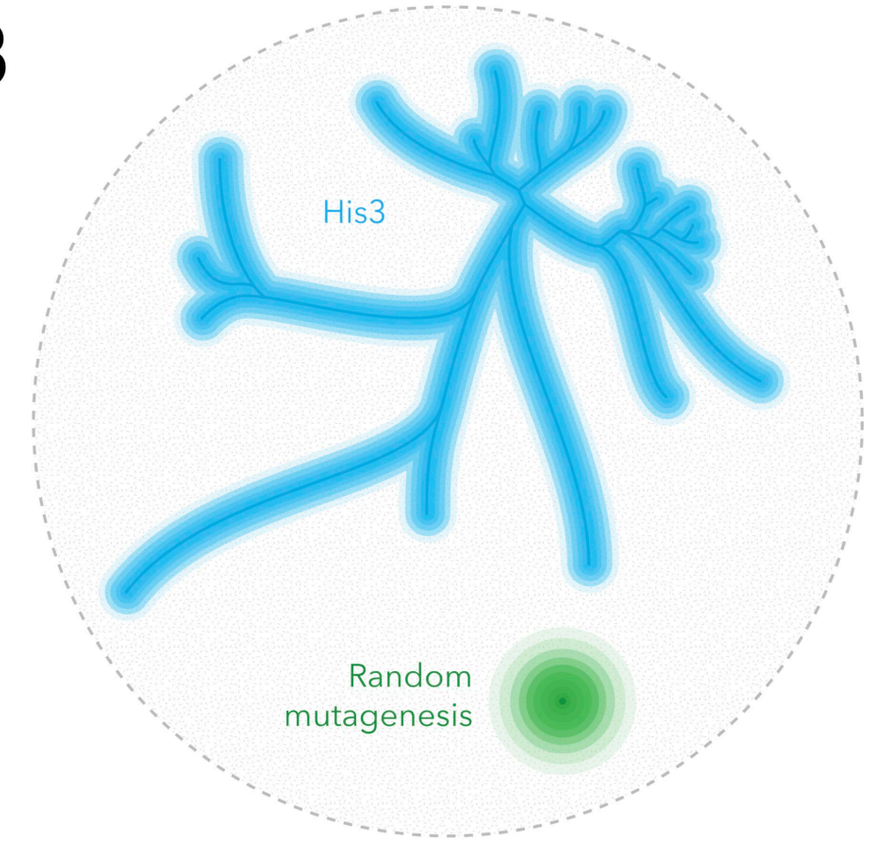
B
His3
Random
mutagenesis

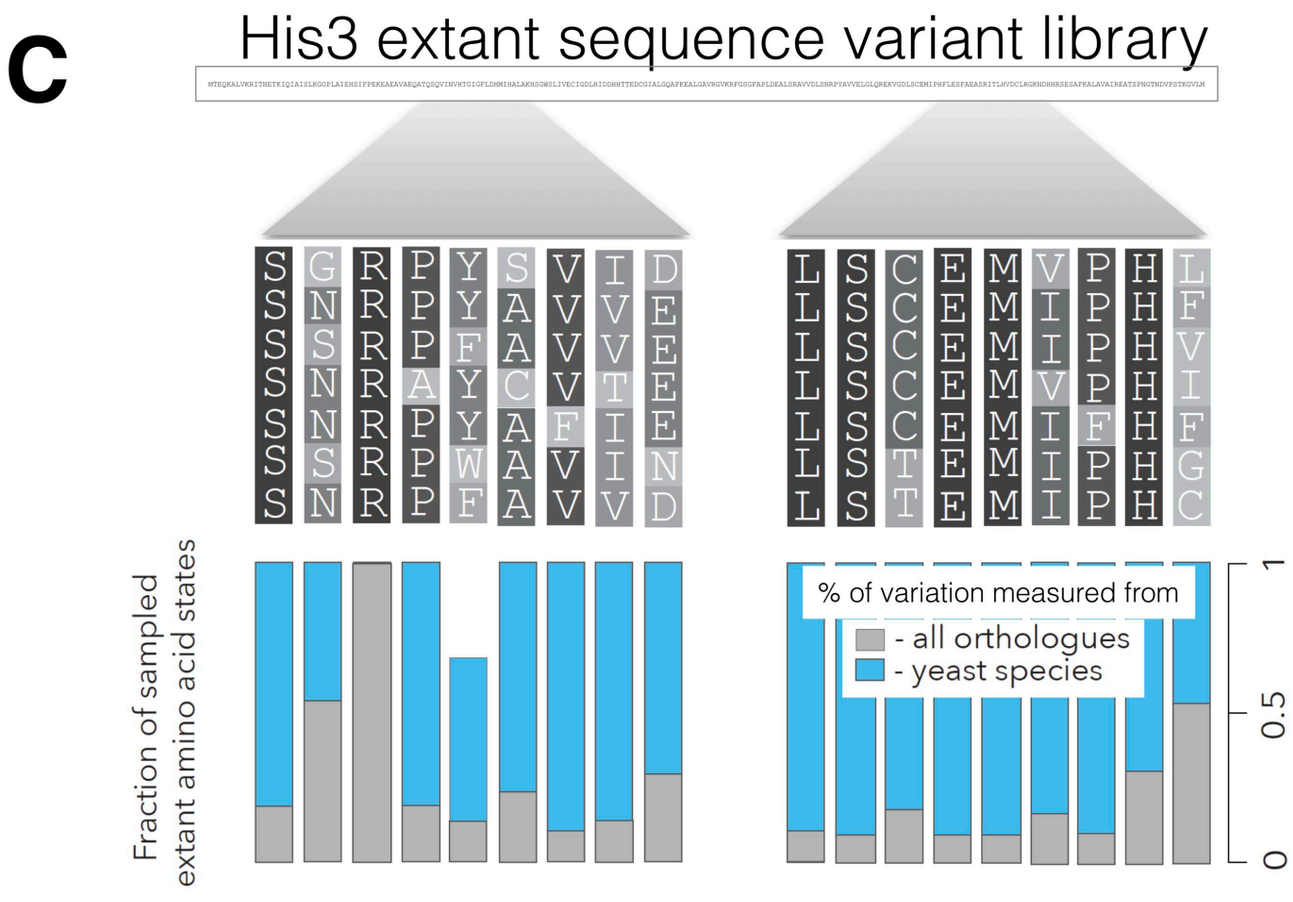
C
His3 extant sequence variant library
Fraction of sampled
extant amino acid states
% of variation measured from
- all orthologues
- yeast species
0
0.5
1

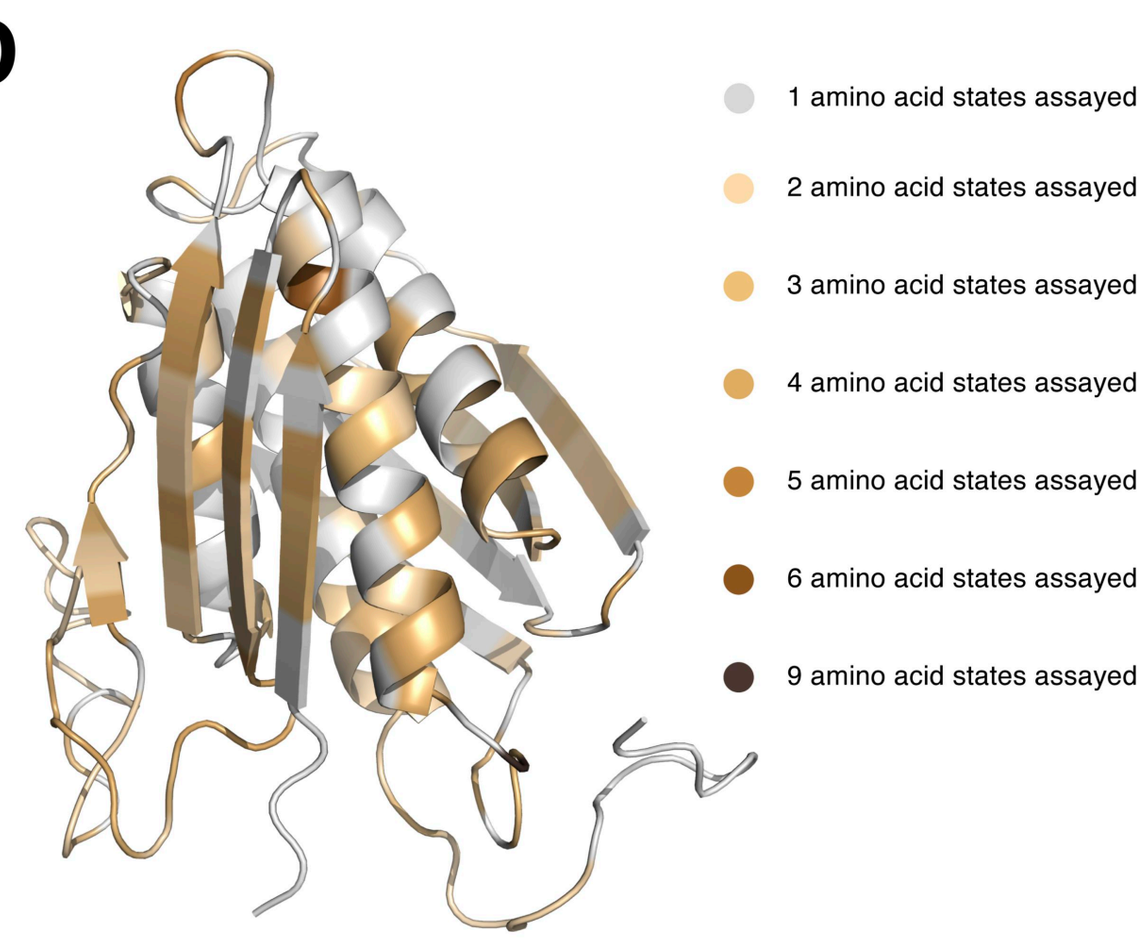
D
1 amino acid states assayed
2 amino acid states assayed
3 amino acid states assayed
4 amino acid states assayed
5 amino acid states assayed
6 amino acid states assayed
9 amino acid states assayed

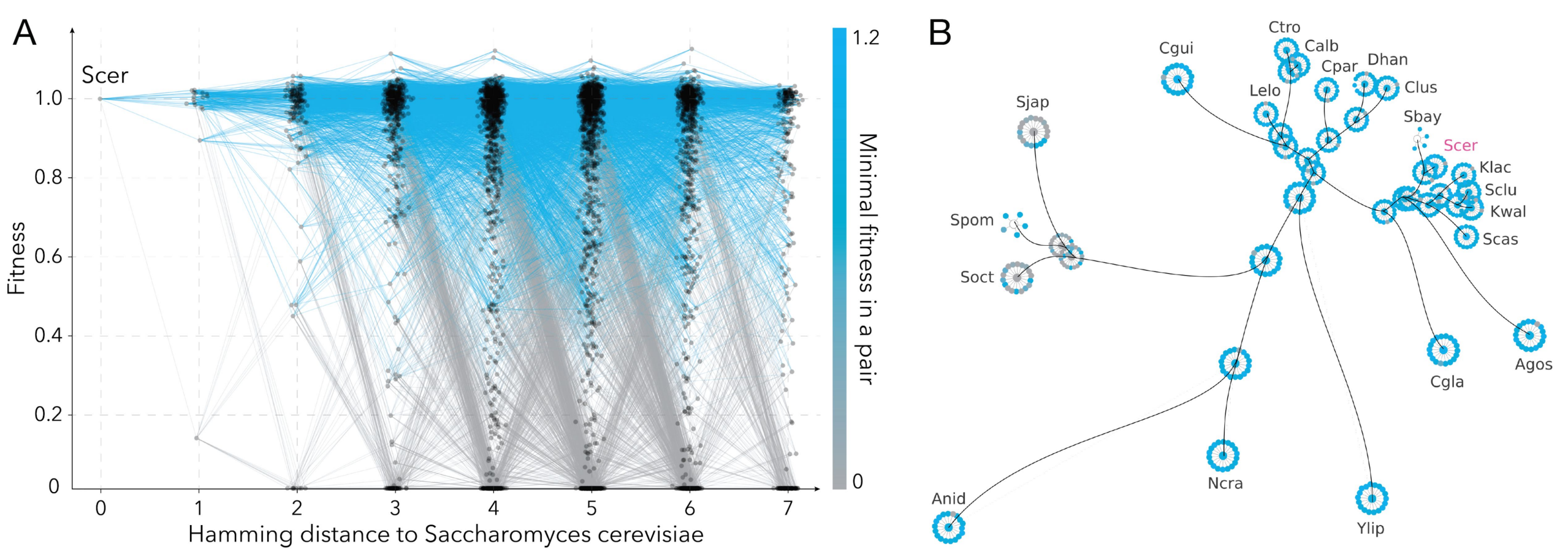
A
Scer
Fitness
1.0
0.8
0.6
0.4
0.2
0
0
1
2
3
4
5
6
7
Hamming distance to Saccharomyces cerevisiae
1.2
Minimal fitness in a pair
0
B
Ctro
Calb
Cgui
Cpar
Dhan
Clus
Lelo
Sjap
Sbay
Scer
Klac
Sclu
Kwal
Spom
Scas
Soct
Agos
Cgla
Ncra
Anid
Ylip

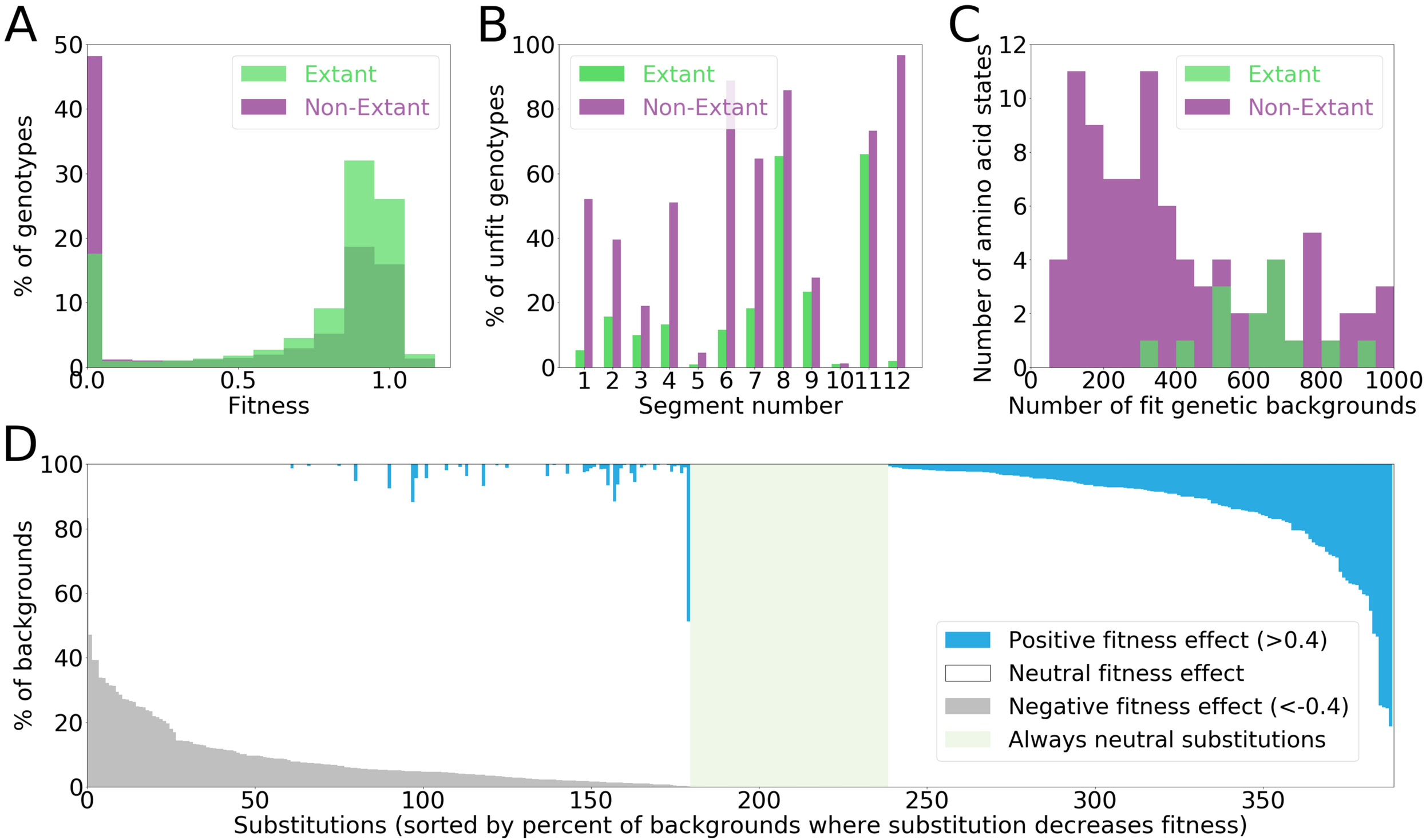
A
% of genotypes
Fitness
Extant
Non-Extant
B
% of unfit genotypes
Segment number
Extant
Non-Extant
C
Number of amino acid states
Number of fit genetic backgrounds
Extant
Non-Extant
D
% of backgrounds
Substitutions (sorted by percent of backgrounds where substitution decreases fitness)
Positive fitness effect (>0.4)
Neutral fitness effect
Negative fitness effect (<-0.4)
Always neutral substitutions

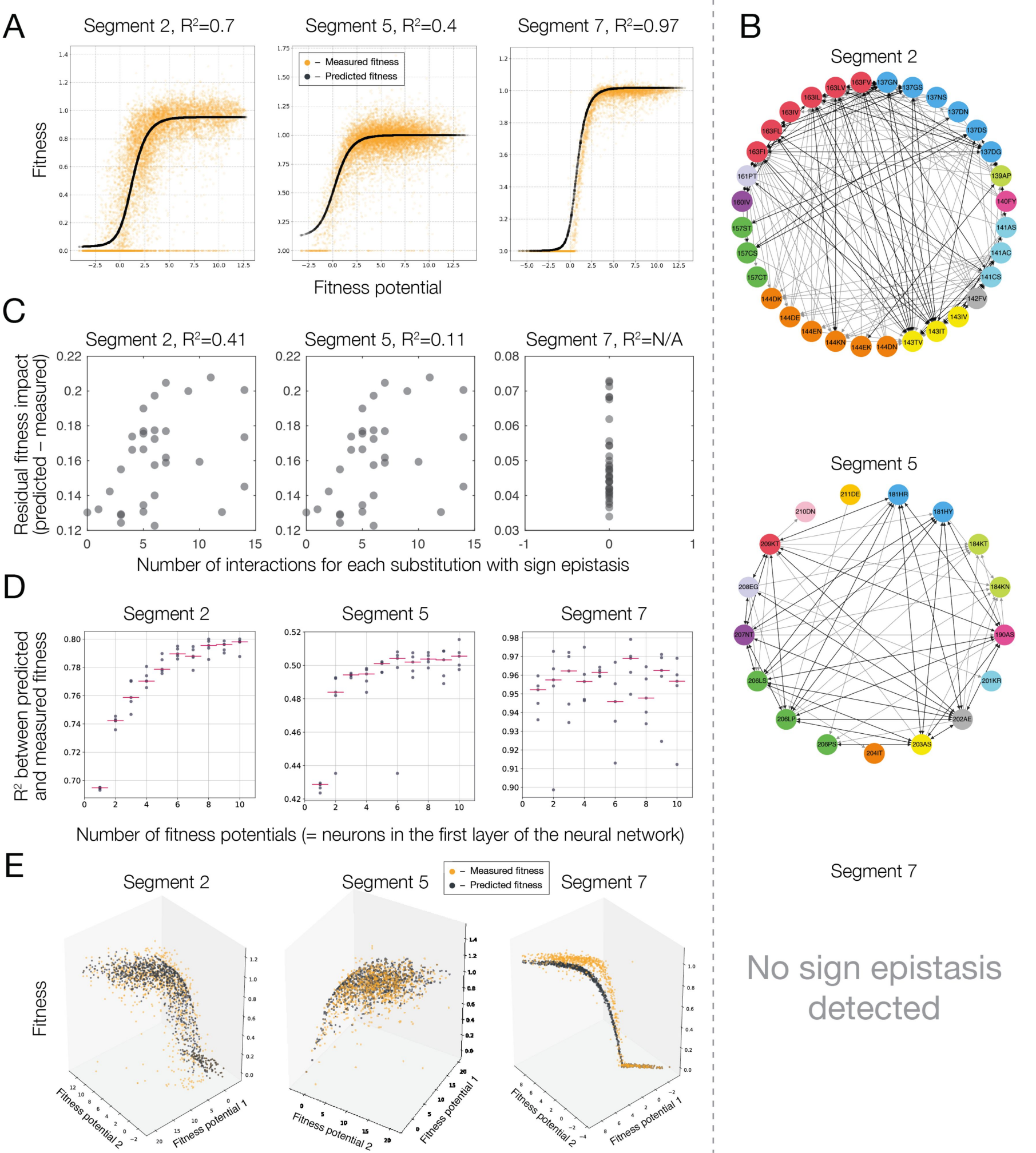
A
Segment 2, R²=0.7
Segment 5, R²=0.4
Segment 7, R²=0.97
Measured fitness
Predicted fitness
Fitness
Fitness potential
B
Segment 2
Segment 5
Segment 7
No sign epistasis detected
C
Segment 2, R²=0.41
Segment 5, R²=0.11
Segment 7, R²=N/A
Residual fitness impact (predicted – measured)
Number of interactions for each substitution with sign epistasis
D
Segment 2
Segment 5
Segment 7
R² between predicted and measured fitness
Number of fitness potentials (= neurons in the first layer of the neural network)
E
Segment 2
Segment 5
Segment 7
Measured fitness
Predicted fitness
Fitness
Fitness potential 1
Fitness potential 2

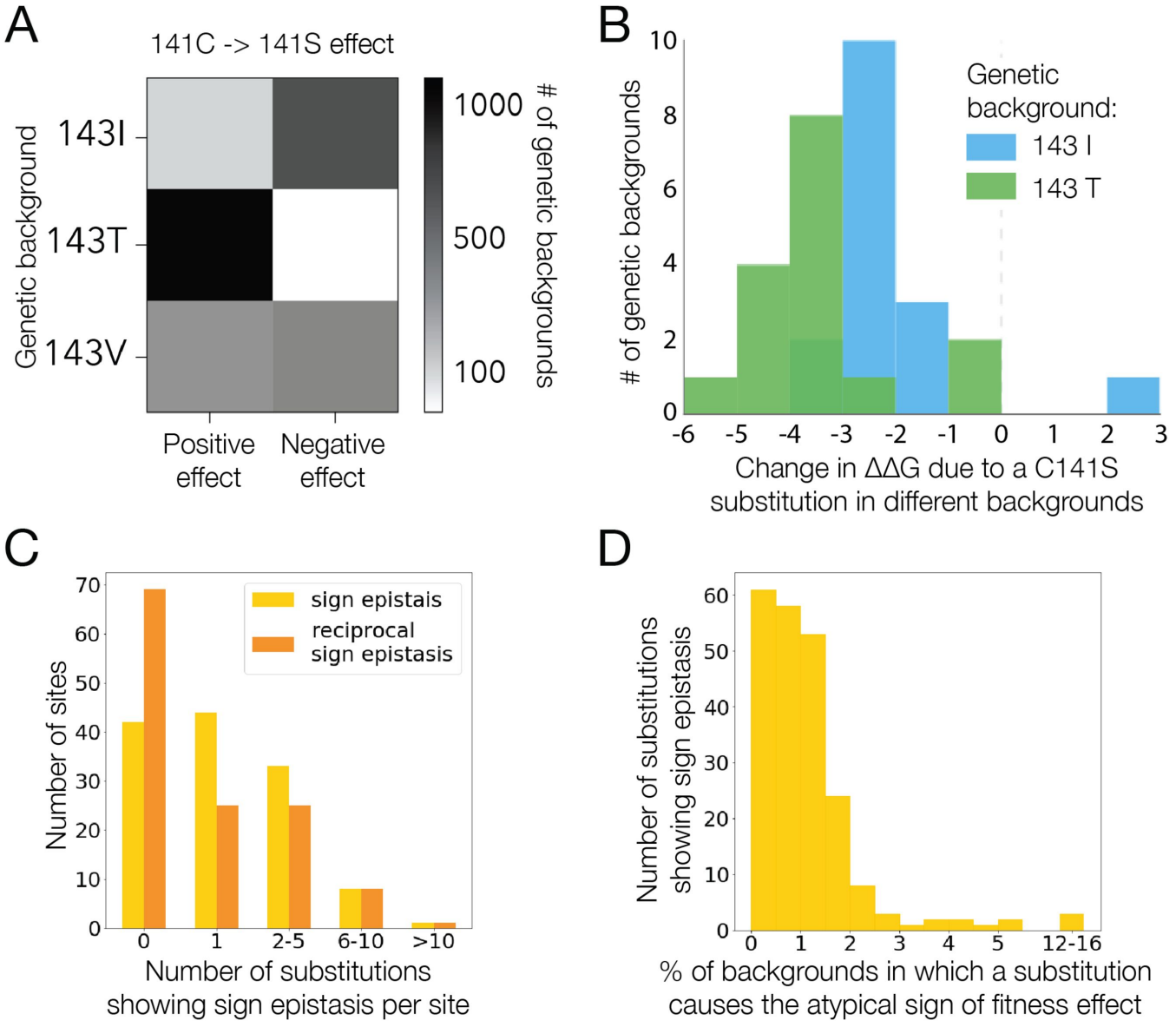
A
141C -> 141S effect
Genetic background
143I
143T
143V
Positive effect
Negative effect
1000
500
100
# of genetic backgrounds
B
# of genetic backgrounds
Genetic background:
143 I
143 T
Change in ΔΔG due to a C141S substitution in different backgrounds
C
Number of sites
sign epistais
reciprocal sign epistasis
0
1
2-5
6-10
>10
Number of substitutions showing sign epistasis per site
D
Number of substitutions showing sign epistasis
12-16
% of backgrounds in which a substitution causes the atypical sign of fitness effect

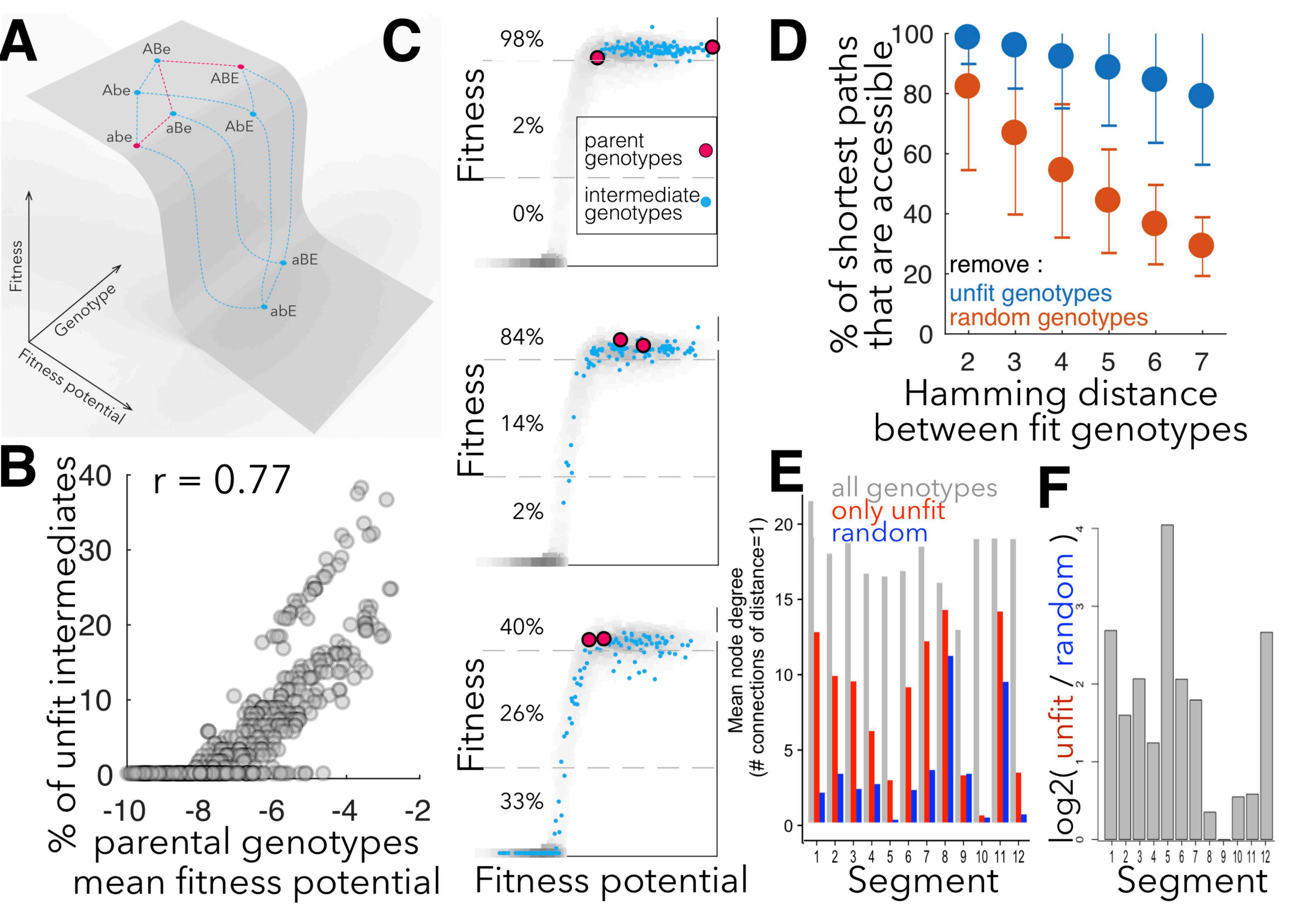
A
ABe
ABE
Abe
abe
aBe
AbE
aBE
abE
Fitness
Genotype
Fitness potential
B
r = 0.77
% of unfit intermediates
40
30
20
10
0
-10
-8
-6
-4
-2
parental genotypes
mean fitness potential
C
98%
2%
0%
Fitness
parent genotypes
intermediate genotypes
84%
14%
2%
Fitness
40%
26%
33%
Fitness
Fitness potential
D
% of shortest paths that are accessible
100
80
60
40
20
0
remove :
unfit genotypes
random genotypes
2
3
4
5
6
7
Hamming distance between fit genotypes
E
all genotypes
only unfit
random
Mean node degree (# connections of distance=1)
20
15
10
5
0
1 2 3 4 5 6 7 8 9 10 11 12
Segment
F
log2(unfit / random)
4
3
2
1
0
1 2 3 4 5 6 7 8 9 10 11 12
Segment

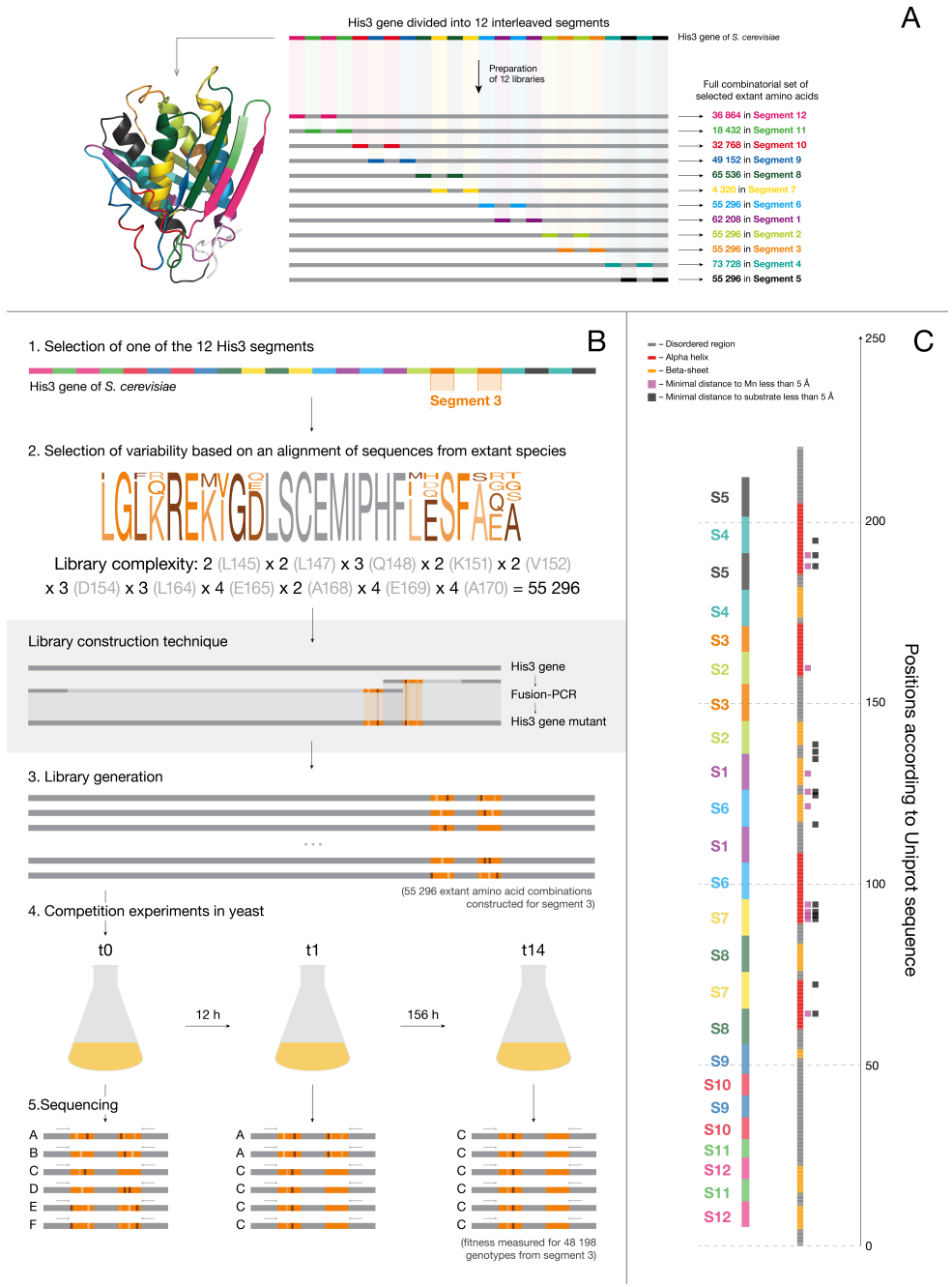
A
His3 gene divided into 12 interleaved segments
His3 gene of S. cerevisiae
Preparation of 12 libraries
Full combinatorial set of selected extant amino acids
36 864 in Segment 12
18 432 in Segment 11
32 768 in Segment 10
49 152 in Segment 9
65 536 in Segment 8
4 320 in Segment 7
55 296 in Segment 6
62 208 in Segment 1
55 296 in Segment 2
55 296 in Segment 3
73 728 in Segment 4
55 296 in Segment 5
B
1. Selection of one of the 12 His3 segments
His3 gene of S. cerevisiae
Segment 3
2. Selection of variability based on an alignment of sequences from extant species
Library complexity: 2 (L145) x 2 (L147) x 3 (Q148) x 2 (K151) x 2 (V152) x 3 (D154) x 3 (L164) x 4 (E165) x 2 (A168) x 4 (E169) x 4 (A170) = 55 296
Library construction technique
His3 gene
Fusion-PCR
His3 gene mutant
3. Library generation
(55 296 extant amino acid combinations constructed for segment 3)
4. Competition experiments in yeast
t0
t1
t14
12 h
156 h
5.Sequencing
(fitness measured for 48 198 genotypes from segment 3)
C
– Disordered region
– Alpha helix
– Beta-sheet
– Minimal distance to Mn less than 5 Å
– Minimal distance to substrate less than 5 Å
Positions according to Uniprot sequence

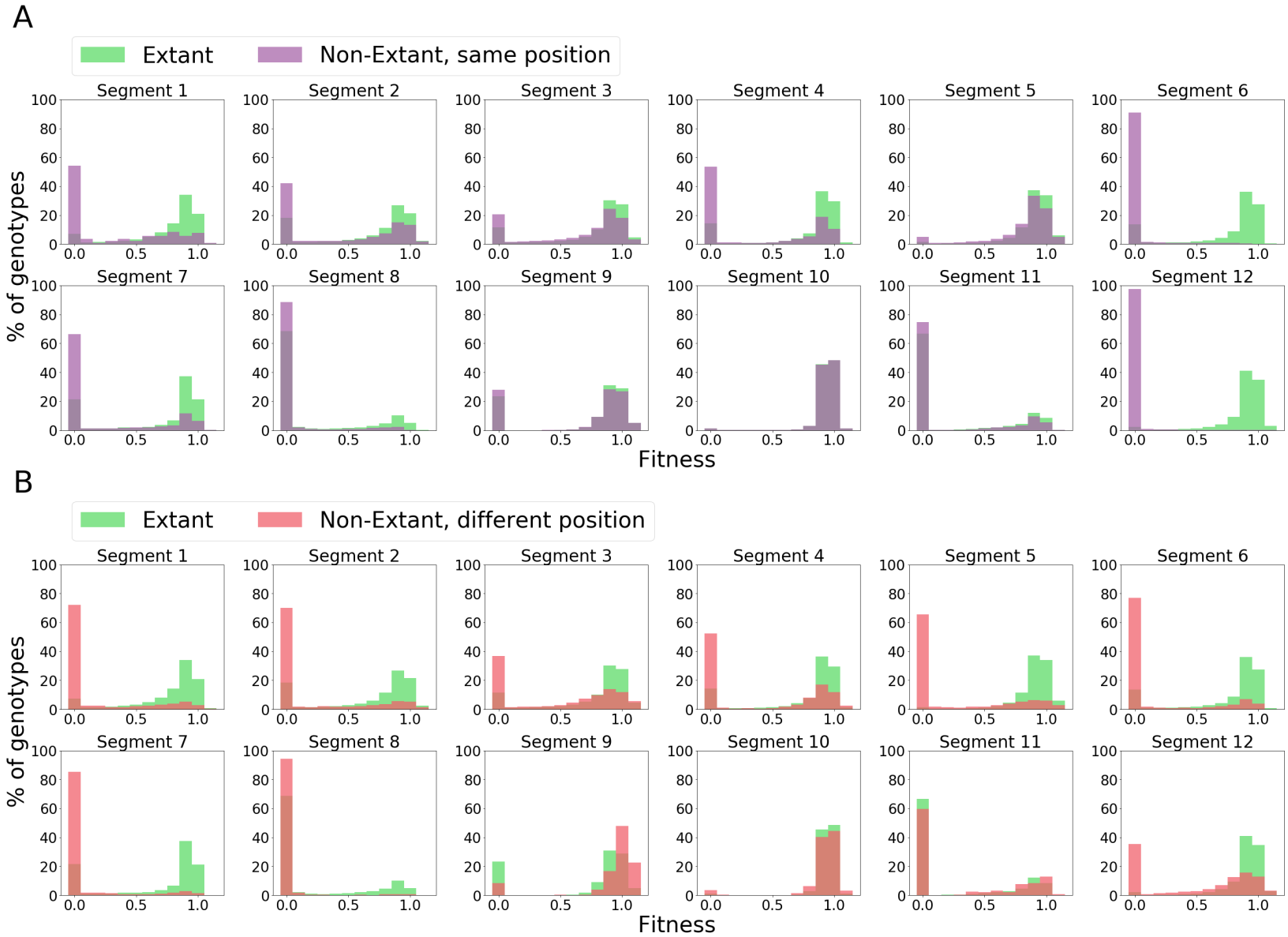
A
Extant
Non-Extant, same position
Segment 1
Segment 2
Segment 3
Segment 4
Segment 5
Segment 6
Segment 7
Segment 8
Segment 9
Segment 10
Segment 11
Segment 12
% of genotypes
Fitness
B
Extant
Non-Extant, different position
Segment 1
Segment 2
Segment 3
Segment 4
Segment 5
Segment 6
Segment 7
Segment 8
Segment 9
Segment 10
Segment 11
Segment 12
% of genotypes
Fitness

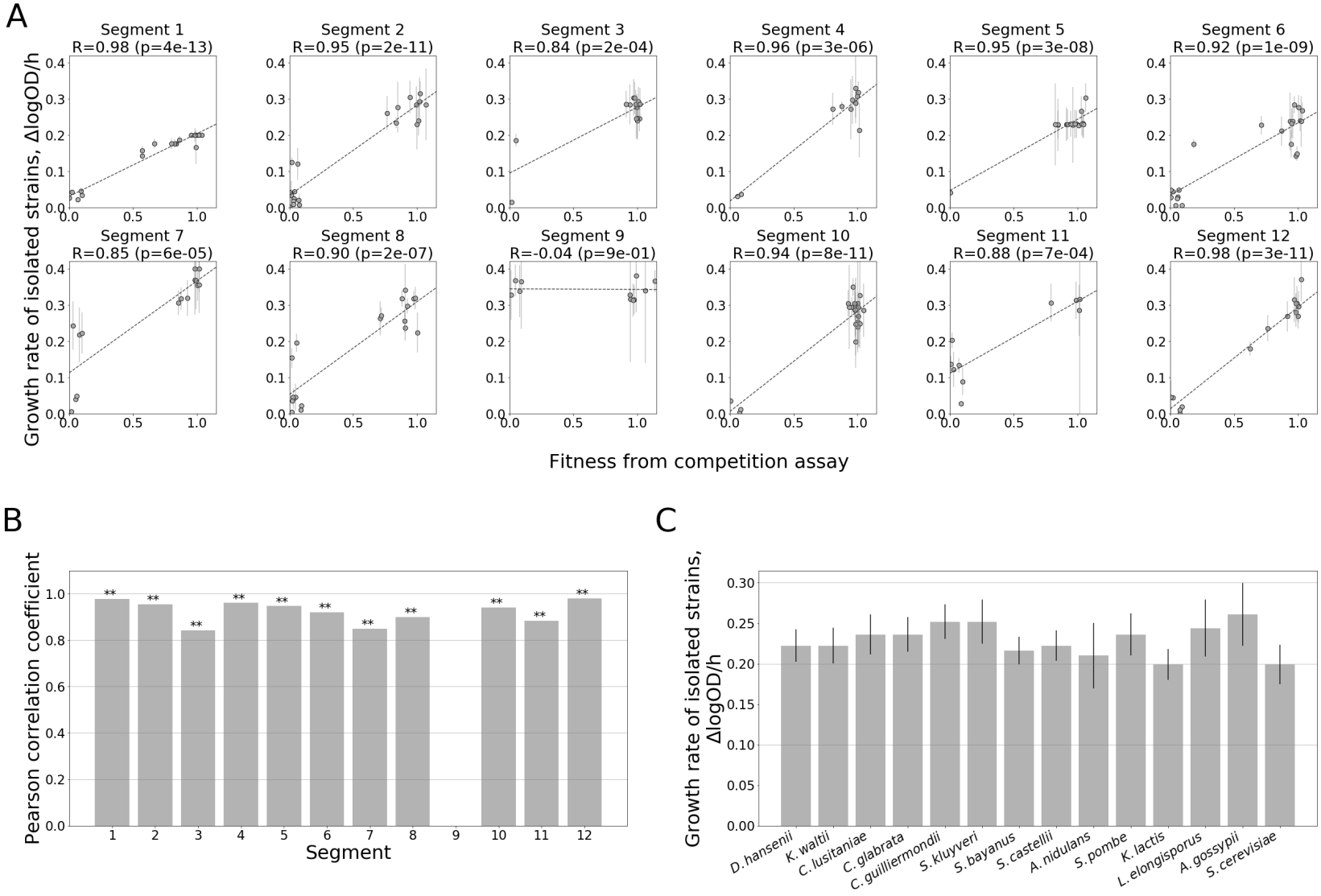
A
Segment 1
R=0.98 (p=4e-13)
Segment 2
R=0.95 (p=2e-11)
Segment 3
R=0.84 (p=2e-04)
Segment 4
R=0.96 (p=3e-06)
Segment 5
R=0.95 (p=3e-08)
Segment 6
R=0.92 (p=1e-09)
Segment 7
R=0.85 (p=6e-05)
Segment 8
R=0.90 (p=2e-07)
Segment 9
R=-0.04 (p=9e-01)
Segment 10
R=0.94 (p=8e-11)
Segment 11
R=0.88 (p=7e-04)
Segment 12
R=0.98 (p=3e-11)
Growth rate of isolated strains, ΔlogOD/h
Fitness from competition assay
B
Pearson correlation coefficient
Segment
C
Growth rate of isolated strains, ΔlogOD/h
D.hansenii
K.waltii
C.lusitaniae
C.glabrata
C.guilliermondii
S.kluyveri
S.bayanus
S.castellii
A.nidulans
S.pombe
K.lactis
L.elongisporus
A.gossypii
S.cerevisiae

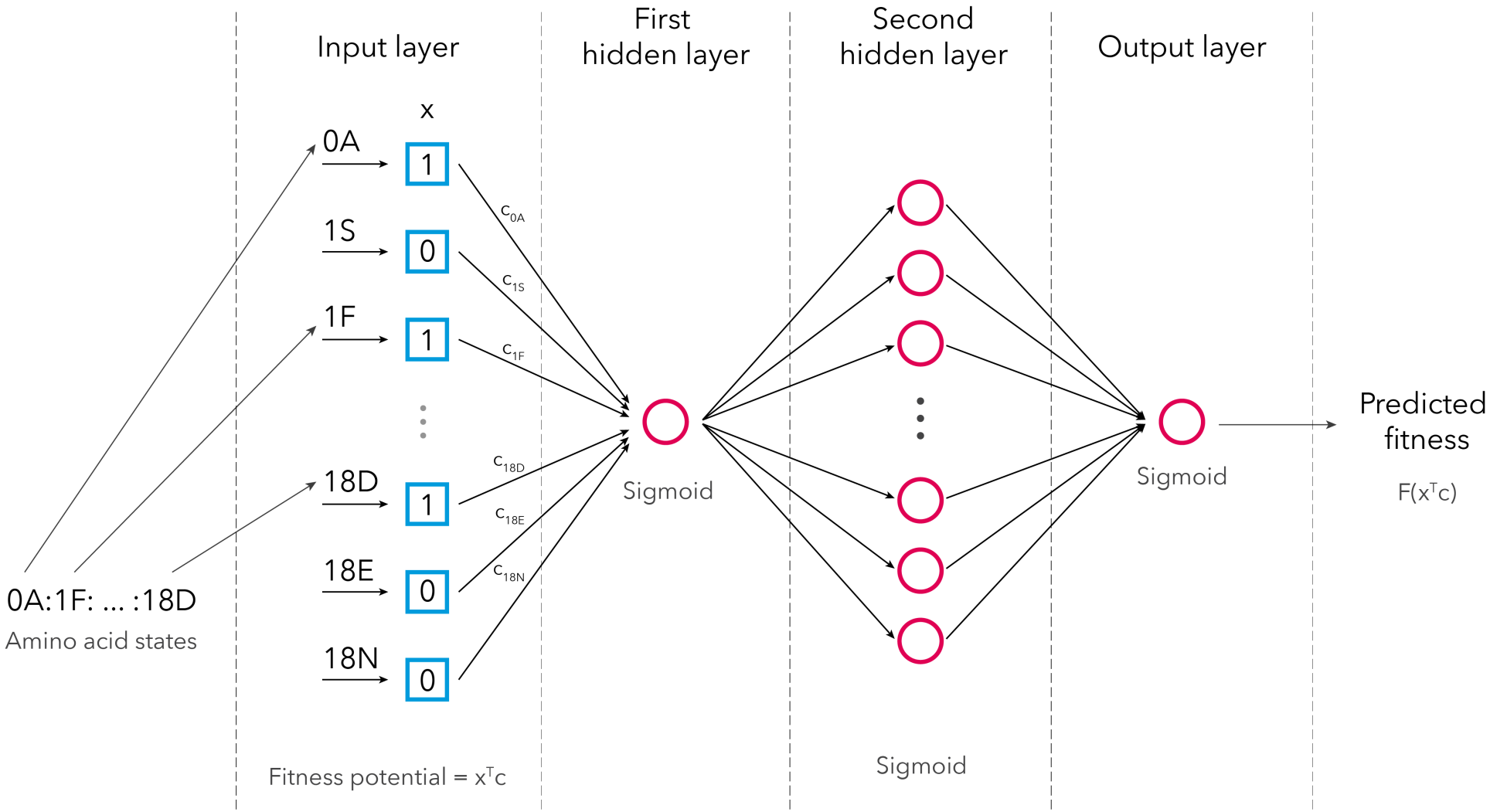
Input layer
First hidden layer
Second hidden layer
Output layer
x
0A
1S
1F
18D
18E
18N
1
0
1
1
0
0
c_{0A}
c_{1S}
c_{1F}
c_{18D}
c_{18E}
c_{18N}
Sigmoid
Sigmoid
Sigmoid
Predicted fitness
$F(x^Tc)$
0A:1F: ... :18D
Amino acid states
Fitness potential = x^Tc

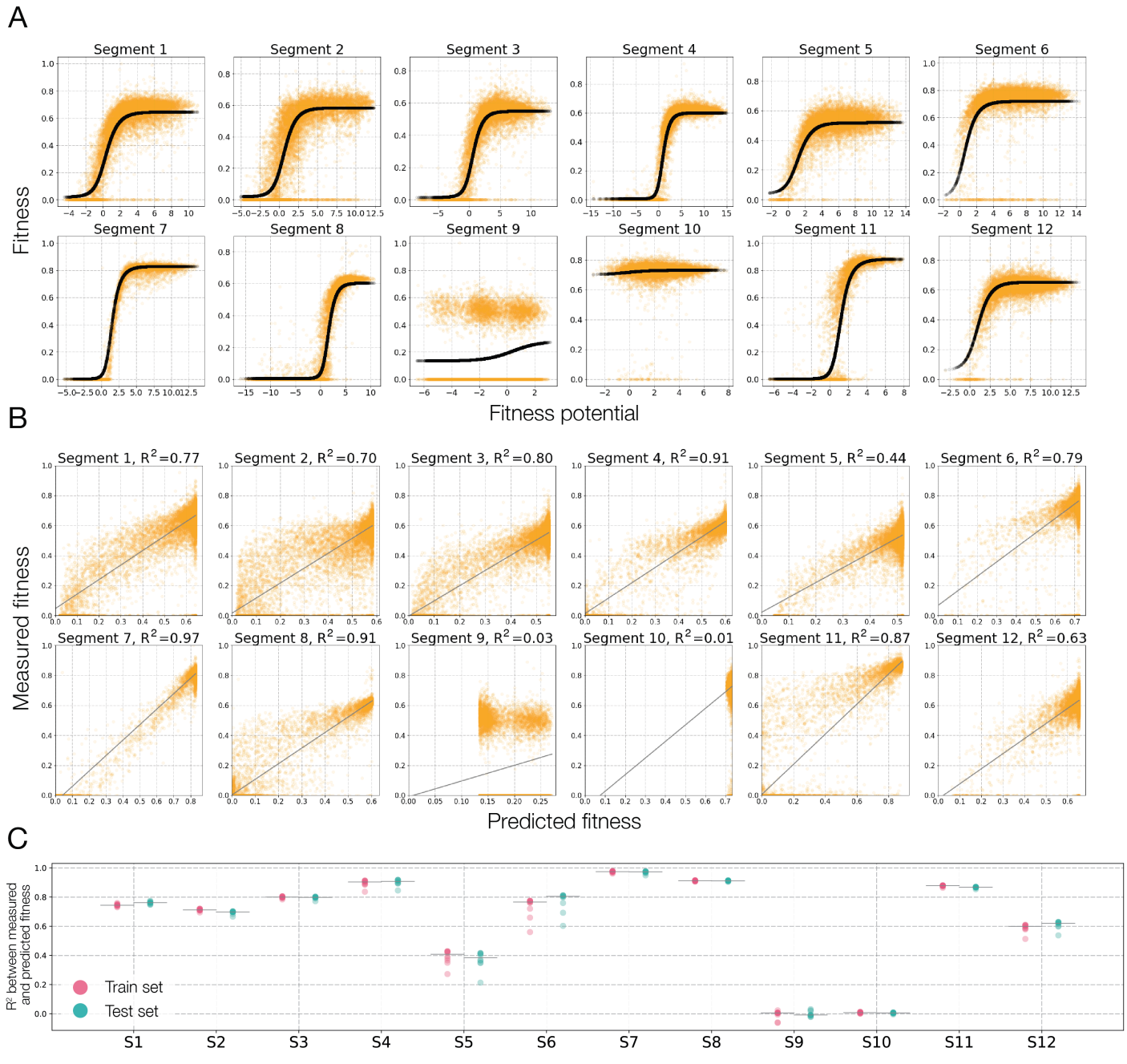
A
Segment 1
Segment 2
Segment 3
Segment 4
Segment 5
Segment 6
Segment 7
Segment 8
Segment 9
Segment 10
Segment 11
Segment 12
Fitness
Fitness potential
B
Segment 1, R²=0.77
Segment 2, R²=0.70
Segment 3, R²=0.80
Segment 4, R²=0.91
Segment 5, R²=0.44
Segment 6, R²=0.79
Segment 7, R²=0.97
Segment 8, R²=0.91
Segment 9, R²=0.03
Segment 10, R²=0.01
Segment 11, R²=0.87
Segment 12, R²=0.63
Measured fitness
Predicted fitness
C
R² between measured and predicted fitness
Train set
Test set
S1
S2
S3
S4
S5
S6
S7
S8
S9
S10
S11
S12

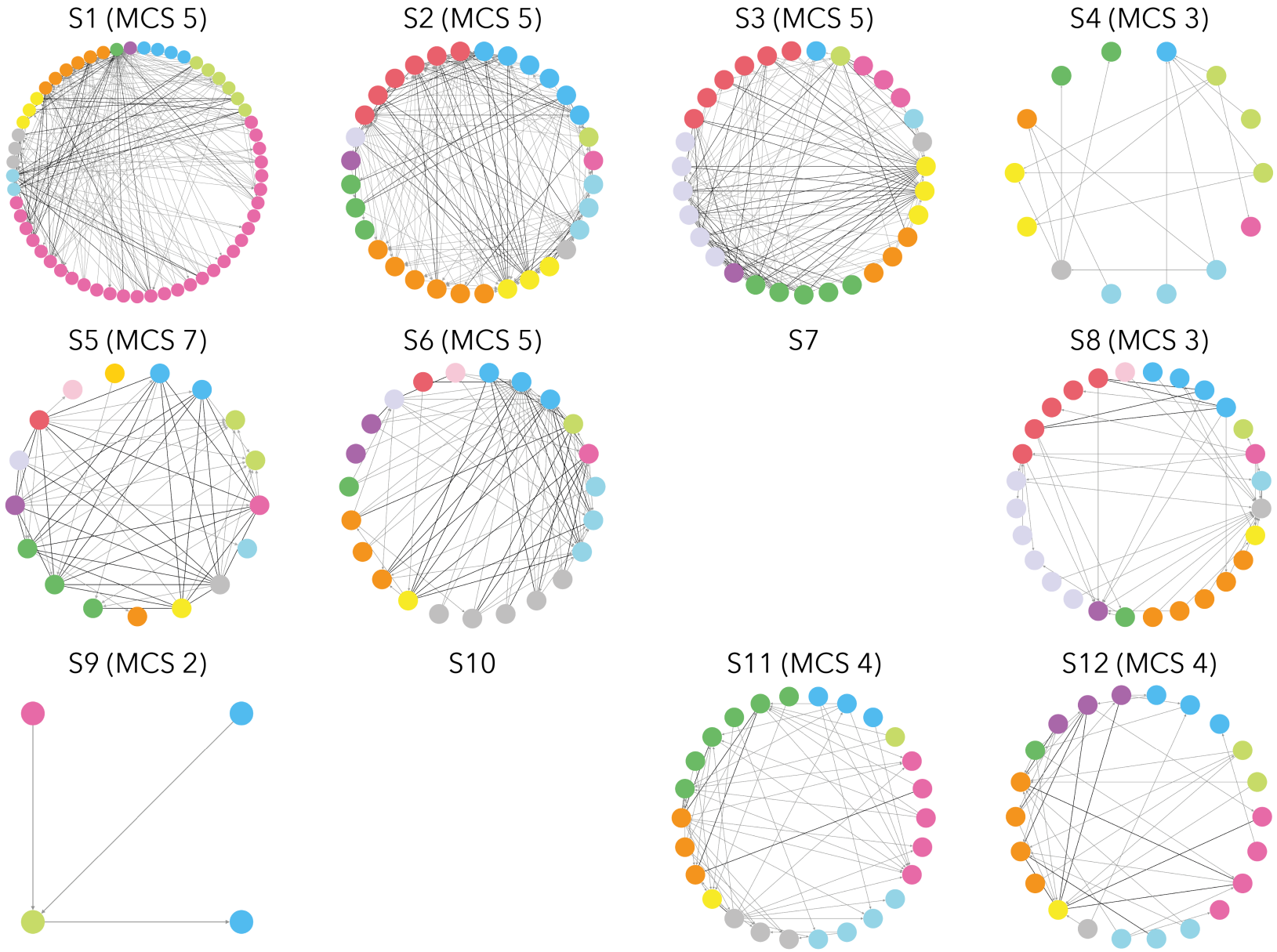
S1 (MCS 5)
S2 (MCS 5)
S3 (MCS 5)
S4 (MCS 3)
S5 (MCS 7)
S6 (MCS 5)
S7
S8 (MCS 3)
S9 (MCS 2)
S10
S11 (MCS 4)
S12 (MCS 4)

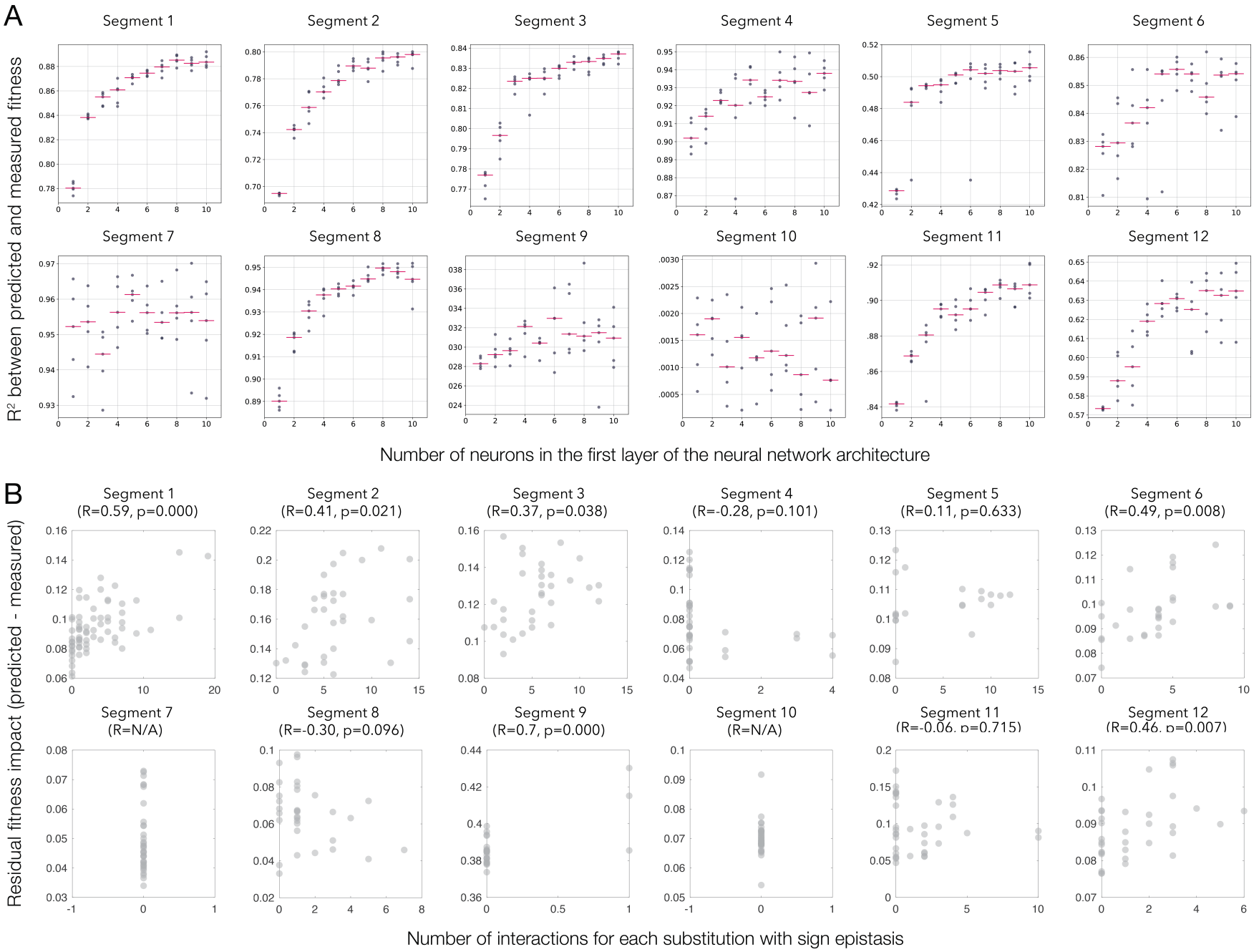
A
Segment 1
Segment 2
Segment 3
Segment 4
Segment 5
Segment 6
Segment 7
Segment 8
Segment 9
Segment 10
Segment 11
Segment 12
R² between predicted and measured fitness
Number of neurons in the first layer of the neural network architecture
B
Segment 1 (R=0.59, p=0.000)
Segment 2 (R=0.41, p=0.021)
Segment 3 (R=0.37, p=0.038)
Segment 4 (R=-0.28, p=0.101)
Segment 5 (R=0.11, p=0.633)
Segment 6 (R=0.49, p=0.008)
Segment 7 (R=N/A)
Segment 8 (R=-0.30, p=0.096)
Segment 9 (R=0.7, p=0.000)
Segment 10 (R=N/A)
Segment 11 (R=-0.06, p=0.715)
Segment 12 (R=0.46, p=0.007)
Residual fitness impact (predicted - measured)
Number of interactions for each substitution with sign epistasis

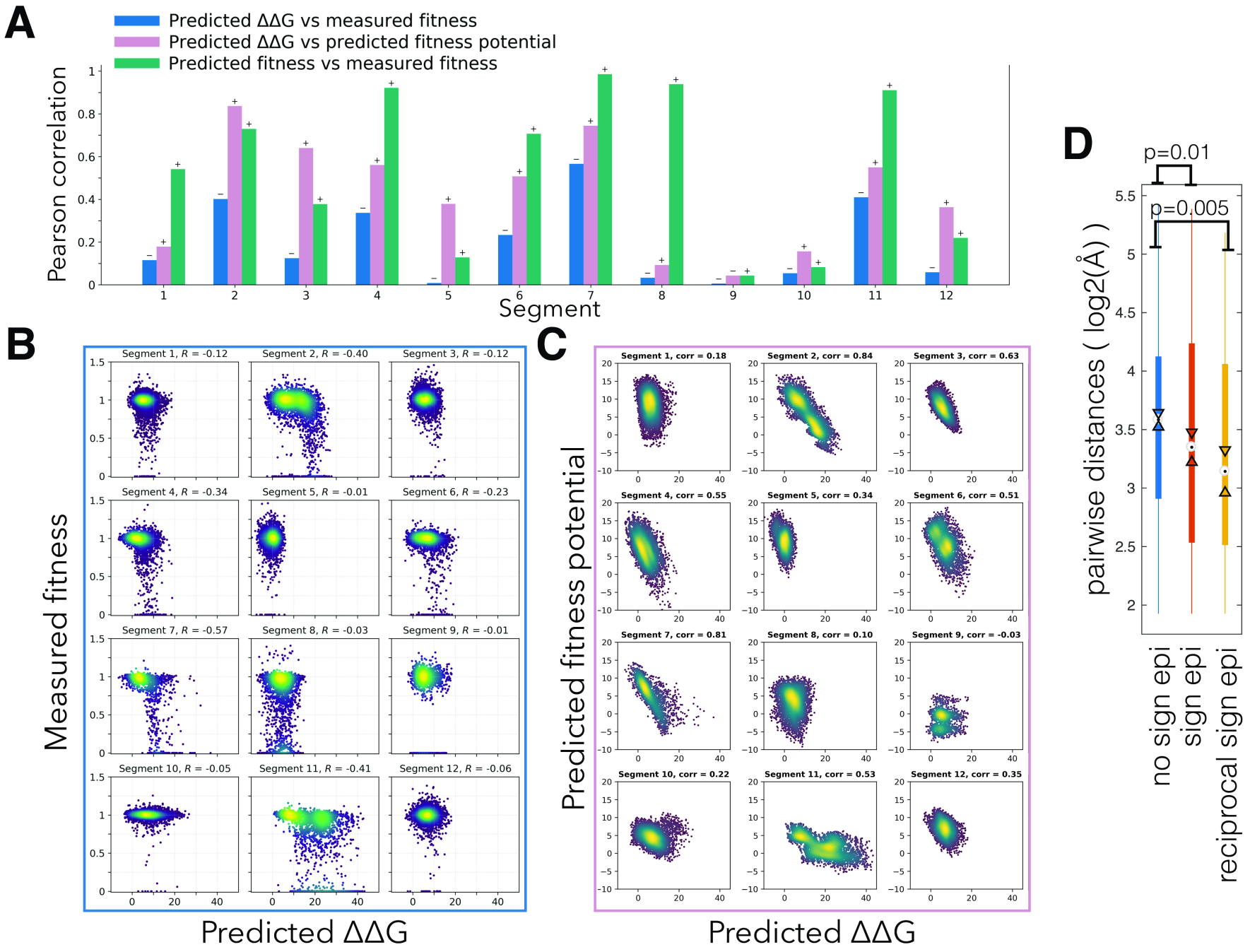
A
Predicted ΔΔG vs measured fitness
Predicted ΔΔG vs predicted fitness potential
Predicted fitness vs measured fitness
Pearson correlation
Segment
B
Measured fitness
Predicted ΔΔG
Segment 1, R = -0.12
Segment 2, R = -0.40
Segment 3, R = -0.12
Segment 4, R = -0.34
Segment 5, R = -0.01
Segment 6, R = -0.23
Segment 7, R = -0.57
Segment 8, R = -0.03
Segment 9, R = -0.01
Segment 10, R = -0.05
Segment 11, R = -0.41
Segment 12, R = -0.06
C
Predicted fitness potential
Predicted ΔΔG
Segment 1, corr = 0.18
Segment 2, corr = 0.84
Segment 3, corr = 0.63
Segment 4, corr = 0.55
Segment 5, corr = 0.34
Segment 6, corr = 0.51
Segment 7, corr = 0.81
Segment 8, corr = 0.10
Segment 9, corr = -0.03
Segment 10, corr = 0.22
Segment 11, corr = 0.53
Segment 12, corr = 0.35
D
p=0.01
p=0.005
pairwise distances (log2(Å))
no sign epi
sign epi
reciprocal sign epi

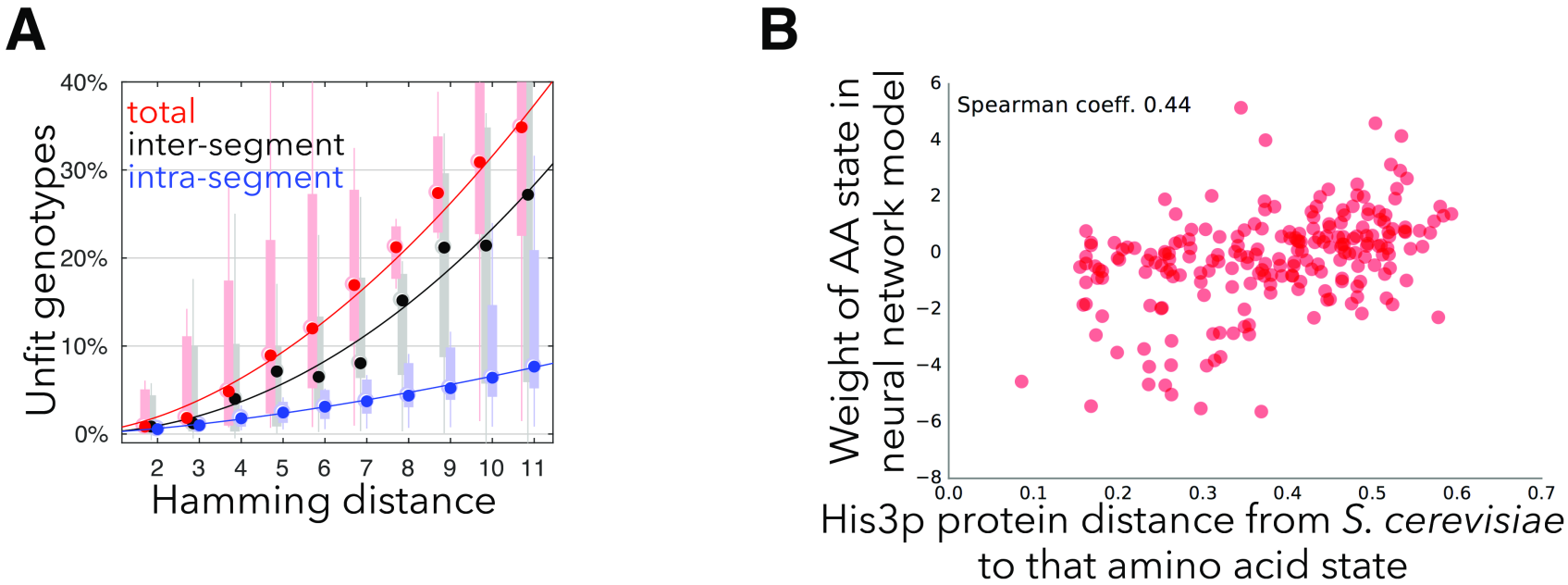
A
40%
30%
20%
10%
0%
Unfit genotypes
total
inter-segment
intra-segment
2 3 4 5 6 7 8 9 10 11
Hamming distance
B
Spearman coeff. 0.44
Weight of AA state in neural network model
6
4
2
0
−2
−4
−6
−8
0.0 0.1 0.2 0.3 0.4 0.5 0.6 0.7
His3p protein distance from S. cerevisiae to that amino acid state